DOKUZ EYLÜL UNIVERSITY
GRADUATE SCHOOL OF NATURAL AND APPLIED SCIENCES

OBTAINING THE THREE-DIMENSIONAL STRUCTURE OF THE CURRENT ENVIRONMENT BY USING FIBER GRATING LASER SYSTEM

by
Emre ÜNSAL

July, 2010
İZMİR

OBTAINING THE THREE-DIMENSIONAL STRUCTURE OF THE CURRENT ENVIRONMENT BY USING FIBER GRATING LASER SYSTEM

A Thesis Submitted to the
Graduate School of Natural and Applied Sciences of Dokuz Eylül University
In Partial Fulfillment of the Requirements for the Degree of Master of Science
in Computer Engineering, Computer Engineering Program

by
Emre ÜNSAL

July, 2010
İZMİR

M.Sc. THESIS EXAMINATION RESULT FORM

We have read the thesis entitle "**OBTAINING THE THREE-DIMENSIONAL STRUCTURE OF THE CURRENT ENVIRONMENT BY USING FIBER GRATING LASER SYSTEM**" completed by **EMRE ÜNSAL** under supervision of **PROF. DR. YALÇIN ÇEBİ** and we certify that in our opinion it is fully adequate, in scope and in quality, as a thesis for the degree of Master of Science.

.....

Prof. Dr. Yalçın ÇEBİ

Supervisor

_____	_____
_____	_____
(Jury Member)	(Jury Member)

_____

Prof.Dr. Mustafa SABUNCU

Director

Graduate School of Natural and Applied Sciences

ACKNOWLEDGMENTS

The author extends his sincere thanks to his supervisor Prof. Dr. Yalçın ÇEBİ for his advice and guidance. The author also thanks to Mustafa KAYABAŞI for his helps and valuable suggestions. This article has been produced through a master degree thesis to Graduate School of Natural and Applied Sciences, Dokuz Eylül University, and this study has been supported as a TUBİTAK (Scientific Research Project). The project number is 108E156 and the name of this TUBİTAK Project is "Eğrisel Ayna ve Matris Desenli Lazer Noktalar Kullanarak Çevrenin Üç Boyutlu Yapısını Oluşturan Tümyönlü (Omni-Directional) Bir Görüntüleme Sisteminin Geliştirilmesi".

Emre ÜNSAL

OBTAINING THE THREE-DIMENSIONAL STRUCTURE OF THE CURRENT ENVIRONMENT BY USING FIBER GRATING LASER SYSTEM

ABSTRACT

It is a necessity that the mobile robots should determine first the obstacles in the environment in which they are located, and then depending on their dimensions, the free areas between the obstacles. For this aim, determination of the mobile robots position is a necessity. In order to find the position of the mobile robot and the locations of the obstacles around it, systems which sense the environment with the help of the camera and provide facilities for self guidance of the mobile robot, were developed based on the development of information technologies.

In the scope of this project, an omnidirectional vision system, which can be used for mobile robots and was intended to determine both the obstacles in the environment and the places through which a mobile robot can pass, by sensing the environment in a three dimensional manner, was developed. During the experiments carried out by using both the mathematical model developed to reduce the errors occurred from the hardware used in the system, and the developed software based on this model, much wider three dimensional structure of the environment was obtained, when compared with classical cameras.

It was seen that, the error rates in the developed system was remained under 10% for all three coordinate axes. Since the location computations are continuously carried out by using the images taken consecutively, and the error rates are acceptable for the close distances, it was seen that this system can be used in mobile robots.

Key words : Fiber Grating; Curved mirror; Omni-directional vision; Stereo imaging; Localization; Three dimensional structure; Image processing

BULUNULAN ORTAMIN ÜÇ BOYUTLU YAPISININ FİBER IZGARALI LAZER SİSTEMİ KULLANILARAK ELDE EDİLMESİ

ÖZ

Gezgin robotların, öncelikle içinde bulundukları ortamdaki engelleri, daha sonra bu engeller arasından, kendi büyüklüklerine göre, geçebilecekleri yerleri belirlemeleri gerekmektedir. Bu amaca yönelik olarak, robotun kendi bulunduğu konumu da belirlemesi zorunluluktur. Gerek robotun kendi konumunu, gerekse de çevresindeki engellerin konumunu belirlemesi için, bilişim teknolojilerinin gelişimine bağlı olarak, kamera ile ortamı algılayan ve robotun kendisini yönlendirilmesine olanak sağlayan sistemler geliştirilmiştir.

Bu proje kapsamında, gezgin robotlar için kullanılabilecek, çevrenin üçboyutlu olarak algılanması sonucunda hem ortamdaki engellerin hem de gezgin robotun geçebileceği yerlerin belirlenmesine yönelik, eğrisel ayna ve matris desenli lazer noktaların kullanıldığı, tümyönlü bir görüntüleme sistemi geliştirilmiştir. Sistemde kullanılan donanımlardan kaynaklanan hataların giderilmesi için geliştirilen matematik model ve bu modele dayanılarak geliştirilen yazılım kullanılarak yapılan denemelerde, klasik kameralara oranla çok daha geniş bir bölgenin üç boyutlu yapısı elde edilmiştir.

Geliştirilen sistemdeki hata oranları, her üç eksen için de %10'un altında kalmıştır. Bu sistemin gezgin robotlarda, ardışık görüntü alımları ile sürekli konum hesaplamaları yapılması ve yakın mesafelerde hata oranlarının kabul edilebilir olması nedeniyle, kullanılabileceği görülmüştür.

Anahtar sözcükler : Fiber Izgara, Eğrisel ayna; Tümyönlü görüntüleme; Stereo görüntüleme; Konumlanma; Üçboyutlu yapı; Görüntü işleme.

CONTENTS

Page

CHAPTER ONE
INTRODUCTION

In robotics, localization and mapping are two most important topics, relating to where the robot is and where to go respectively. Localization is the operation of determining the place or point that the mobile robot is standing according to some reference points in the environment. Mapping is the procedure of obtaining the 2D or 3D structure of the environment in which the mobile robot is present. The route of the mobile robot, which enables secure passing width, is defined as the travelling path. Since the mobile robot position will be changed while travelling on the path, system position information must be updated periodically.

When the mobile robot can identify its position, it becomes easy to identify its direction and distance in mobile robot applications. The position of a point in the environment is determined by using the distance of surrounding objects and their direction (for example, with the angular position) to this point. Since mobile robot's location and the location of the obstacles in the environment can be determined easily by using an imaging system mounted to the mobile robot, it travels more safely on the route.

In omni-directional vision systems, 2D or 3D analysis is made to obtain the structure of the environment. For determination of distances between obstacles and the vision system, it is necessary to model the reflection of the light coming to surface of the curved mirror and the formation of a point of an obstacle in the image plane after the reflection. It is important to construct a mathematical model which is able to measure these distances. A point in the real world should be represented by at least two different perspectives in the images in order to be able to obtain the distance of that point in a stereo system.

In this study, a new vision system which consists of two curved mirrors and two cameras are developed. Since the placement of a pixel (of a real world obstacle) in the surface of one mirror should be compared with the placement in the same pixel in

the surface of the other mirror, two mirrors are needed. Moreover, a mathematical model which is capable of measuring the distance of objects from the vision system is presented.

In order to obtain the localization and mapping information, a dot-matrix laser pattern is obtained by laser source diffracted by a Fiber Grating Device (FGD) (Habib, 2007; Ohya, Shoji & Yuta, 1994). It is scattered to the surrounding environment of the vision system, the image of the environment with the dot-matrix laser pattern is used to determine the distance of obstacles from the vision system and to construct the 3D structures of the obstacles.

The proposed vision system will not only reduce the cost image processing cost but also reduce the cost of 3D construction procedure of the environment.

CHAPTER TWO
RELATED WORKS

2.1 Imaging Systems

Distance measurement has great importance for safe mobile robot navigation. The distance between obstacles in the environment and the mobile robot is calculated, and the robot's location and environment map is identified by using the distance information. In different existing works, it was seen that ultrasound (Gasparri et al., 2007), laser (Duan & Cai, 2008), camera sensors (Kriegman et al., 1989) or hybrid model (Chang et al., 2008) for localization and mapping were used. Since perspective stereo cameras can provide more information of the surrounding environment, they are now widely used. However, they have limited Field Of View (FOV) and matching a pixel pair in two images has some difficulties in stereo visualization such as high computational cost (Wang & Hsiao, 1996).

In order to solve the limited FOV problem, omni-directional vision systems have been used. In these systems, a classical camera with limited FOV is fixed in front of a curved conical, parabolic or hyperbolic mirror. As a result, a wider angle of the environment appears in the curved mirror. Curved mirrors can have up to 180 degree of vertical and 360 degree of horizontal view. This wide FOV can be obtained by a classical camera fixed against a curved mirror. This visualization is called omni-directional and has been widely used especially during last decade (Nayar, 1997; Gluckman & Nayar, 1999; Gluckman & Nayar, 2002). The omni-directional vision is achieved by a curved mirror such as spherical, conical, parabolic or hyperbolic mirror and a conventional camera pair (Baker & Nayer, 1999). Omni-directional vision can view the wide FOV of the surroundings. There is almost no need for rotating the camera and the objects in the environment can always be kept in sight. Such vision systems are used in many fields such as navigation of mobile robots, tracking, localization and mapping, and security systems.

Gluckman, Nayar and Thoresz worked with two parabolic mirrors and two cameras fixed in front of each mirror, and the distance of a point in the real world from the vision system was calculated by triangulation method in a stereo approach manner (Gluckman et al. 1998). Although the two cameras are the same model and type, during the implementation, the alignments of two cameras in the stereo system cannot be exactly the same and so the focal distances don't match. Besides, the differences in imaging receptors (sensors) of these two cameras may lead some differences in the displayed color values of the laser points. Since the image sensors of two cameras may differ, pixel values of a point in two sensors are not exactly the same.

Therefore, to have same characteristics such as response, gain and offset of vision system, a number of studies have suggested the use of a single camera in the stereo systems. In these studies, shapes and number of mirrors may differ. However, the common point in all these studies is that the visualization is obtained from more than one image. In a stereo system with a single camera, the calibration procedure is difficult and the stereo matching is much more complex. In stereo systems pixels of an image in one mirror should be matched with the pixels of an image in the other mirror. This matching procedure is done with image processing algorithms such as Sum of Squared Differences (SSD), Real-Time Correlation-Based Stereo and Dynamic programming, but the cost of the computation and the amount of error are relatively high.

Some studies were also carried out by using Fiber Grating Device (FGD) and classical camera with limited field of view (FOV) to detect obstacles, tracking and 3D construction of the environment. In these studies, a dot-matrix laser pattern is obtained by passing the laser through the FGD. (Yamaguchi & Nakajima, 1990; Habib, 2007; Nakazawa & Suzuki, 1991).

2.2 Omni-Directional Imaging System

In classical computer vision systems, classical stereo cameras are widely used. However, they have limited field of view (FOV). Besides, curved mirrors can reflect the environment at an angle greater than 180 degrees on their own as shown in Figure 2.1. If a perspective stereo camera is placed in front of this curved mirror (Figure 2.1a), it can be possible to view the image of environment on the mirror with a wide angle (Figure 2.1b).

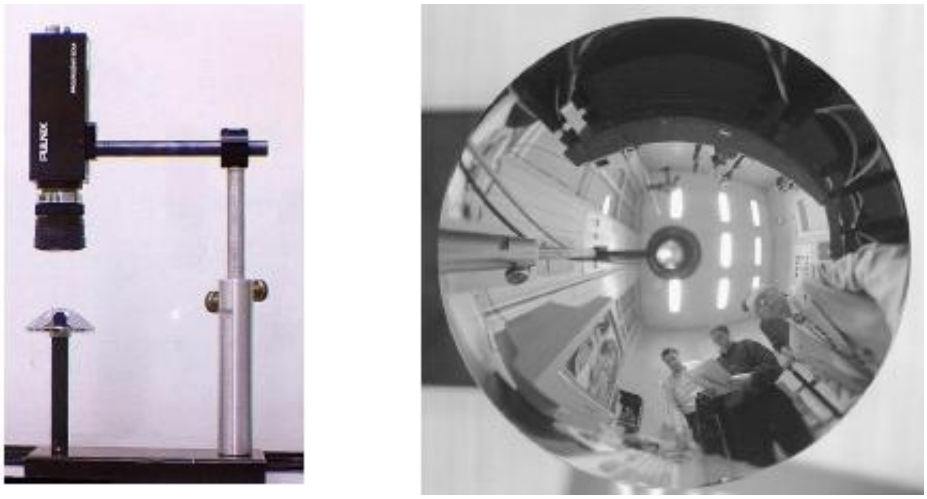

(a) A hyperbolic mirror and perspective camera system

(b) Panoramic view of environment by using the imaging system in figure (a).

Figure 2.1 Hyperbolic mirror previews (Svoboda, Pajdla & Hlavac, 2002).

This omni-directional imaging technique is called "*omnivision*". In this system, A curved mirror and a camera placed in front of the curved mirror is used in this system. Hyperbolic or parabolic curved mirrors are generally used in omni-directional imaging systems.

These mirrors have focal points which determine the direction and reflection angle of the reflected light from these mirrors, and this situation is called "*central projection*".

In curved mirrors with central projection, the focal point is also the center of the curved mirror. The line which connects focal point to the midpoint of image plane is called Y-axis, and the line perpendicular to Y-axis is called X-axis. All evaluations are conducted according to these axes.

In this type of mirrors, all the light beams coming from any points on the environment are reflected from the focal point of the mirror with a particular angle value. One of the curved mirrors with central projection is parabolic mirror. All the reflected light beams from parabolic mirror are parallel with Y-axis as shown in Figure2.2 (Nene & Nayar, 1998).

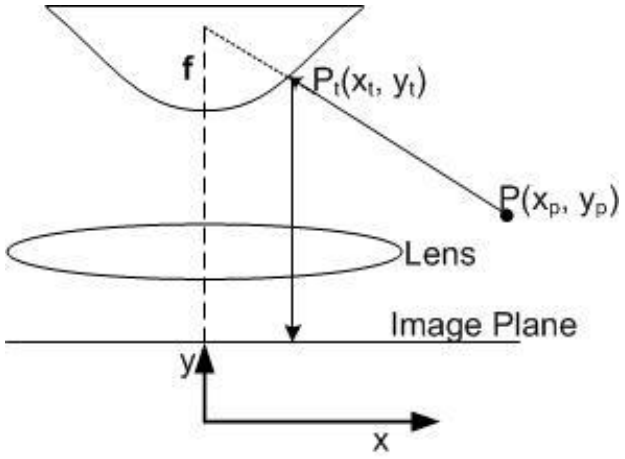

Figure 2.2 Light projection on the image plane in parabolic mirror.

Another type of curved mirrors with central projection is hyperbolic mirror. All the reflected light beams from hyperbolic mirrors have different angle values with Y-axis as shown in Figure 2.3, and these light beams intersect in the focus of the hyperboloid. The center of camera projection coincides with the focus of second mirror. There are also some curved mirrors which do not have central projection, and in these types of mirrors the light reflection from the curved mirror becomes more complicated (Nene & Nayar, 1998).

Omni-directional imaging systems can scan the environment with 360 degree FOV by using curved mirrors. Especially the aim in robotics implementations is not

only to see a large field of view, but also determine the robots where to go and how to go.

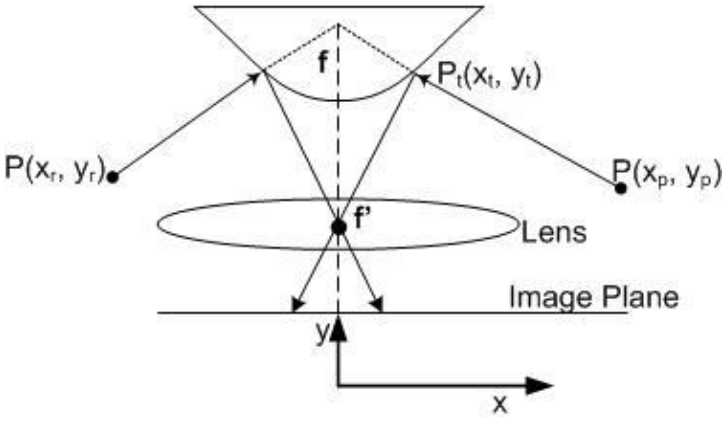

Figure 2.3 Light projection on the image plane in hyperbolic mirror.

When calculating the distance of any point in the environment, a model should be constructed for the reflection of the light in the image plane for any imaging system, and a mathematical model should also be constructed. The constructed model is used to calculate distances, but some mathematical models do not include distance calculation. For example, the reflection of a light beam in the image plane can be modeled for a single camera, but this model does not provide the mathematical model for calculating the distance for the real point in the imaging environment. In order to calculate the distance, a reference point or a benchmark is needed. Therefore, the real distance between two curved mirrors and a real point in the environment is needed to be calculated from the vision system. This type of imaging technique is called "*stereo imaging technique"*.

In stereo imaging systems, an actual point in the environment must be placed in the image plane of both curved mirrors. Finding the equivalent of a point in an image plane in the other mirrors image plane is called "*matching*". When matching images, image processing algorithms and similarity matching algorithms are used, but these algorithms can produce a result in a long time. Moreover, in some cases, the matching process may not work well and wrong points can be matched. This causes significant problems in distance calculation.

CHAPTER THREE
SYSTEM HARDWARE DEVELOPMENT

3.1 Preparing Vision System

3.1.1 Preparing the Initial Vision System Hardware

At the beginning of this project a system with two hyperbolic mirrors with 60 mm radius and a digital camera which has 3.2 Mega pixel resolutions was constructed as the imaging system as shown in Figure 3.1. A holder is also prepared for fixing the camera and mirrors in the vertical axis. The holder allows changing the distance between two hyperbolic mirrors, and the distance between mirrors and the digital camera. Thus it supplies an advance to try various distances for imaging system, and some experiments were experienced by using this imaging system.

Figure 3.1 Initial imaging system.

At the beginning, the image of the mirror on both sides of the camera were taken and analyzed as shown in Figure 3.2. General view of the image of mirror placed left side of the camera and the image of the mirror placed center of the camera are given respectively in Figure 3.2a and 3.2c.

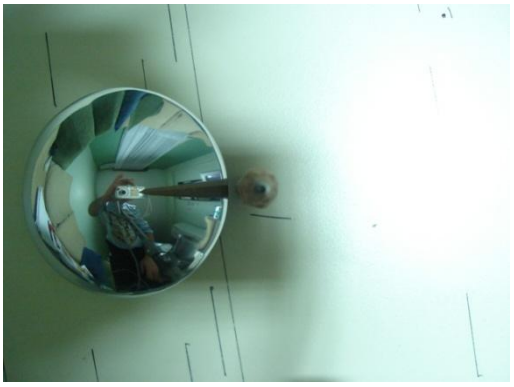

(a) Left Side Image

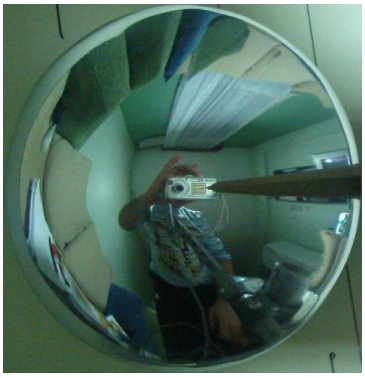

(b) Zoomed Left Side Image

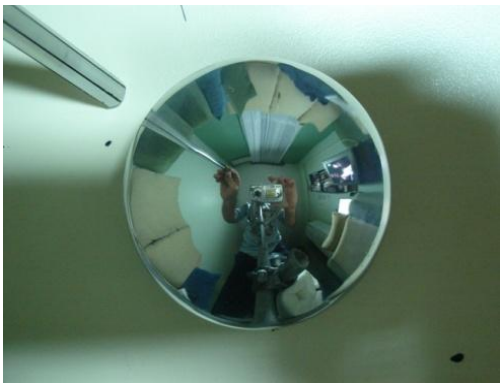

(c) Centered Image

(d) Zoomed Centered Image

Figure 3.2 Images taken from prepared hyperbolic mirrors.

During the analysis, it was seen that when the center of the camera is getting further from the mirror, the distortion of the image is increasing nonlinearly. As a result of the distortion, circular shape of the mirror image changes to an elliptical form as shown in Figure 3.2b. The distortion of the image in the mirror also causes nonlinear distortion of the image of environment. In order to calculate the distortion the images in Figure 3.2b and Figure 3.2d were used. For this purpose the ratio between vertical and horizontal radius for each image was calculated. For the image given in Figure 3.2b, the resolution was 1152x1180 pixels, so the distortion ratio for Figure 3.2b was calculated as;

$$r_b = \frac{1152}{1180} = 0.97627$$

For the image given in Figure 3.2d, the resolution was 1524x1529 pixels, so the distortion ratio for Figure 3.2d was calculated as;

$$r_d = \frac{1524}{1529} = 0.99673$$

Theoretically, the ratio between two axes for a circular mirror must be “1.0”. Although the error ratio for the prepared metallic mirrors was said to be ignorable, the distortion ratio of the image planes for Figure 3.2b and Figure 3.2d were calculated %2.34 and %0.33 respectively, which cause considerable distortion on both images.

Curved mirrors have FOV 360^o with horizontal axis and more than 100^o FOV with vertical axis. So, very large scale of environment can be viewed in a curved mirror having 60mm radius. Since large FOV value exists in a small area, the small distortions on the mirrors may cause large errors on the real image. It was seen that the distortion has increased exponentially with the increasing of the distance between vision system and objects.

Another significant problem was that the occurrences of the same object on both mirrors were quite different of mirrors as given in Figure 3.3. Light beams coming from the objects located in the environment are seen on different points from the center of the each mirror (Figure 3.3b). Using two curved mirrors and one camera which is placed in the center of the two mirrors are given in Figure 3.3a.

The distance between camera axis and one mirror’s image of any point placed in the environment is different from the other mirror’s image of that point (Figure 3.3). While the distance from the camera is changing, the distortion in the mirror image also changes. The equivalent image point on the other mirror image can only be calculated with a significant error rate. In addition to this, these calculated points are placed in different coordinates in the mirror images which is expected.

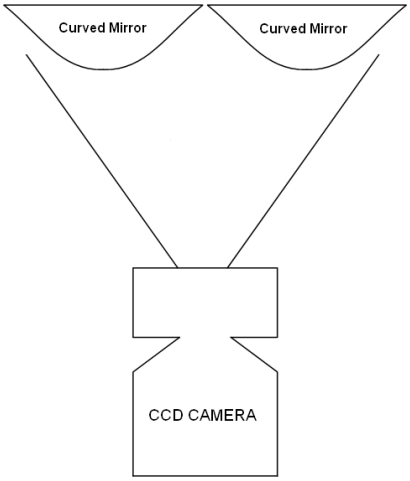

(a) Lateral view of the vision system

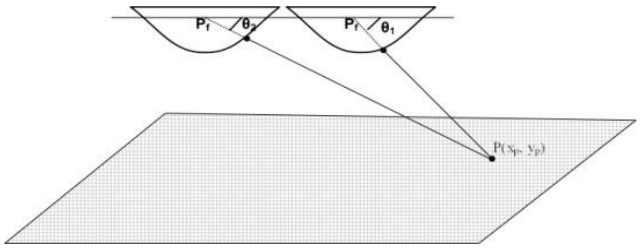

(b) View of a point in the imaging system

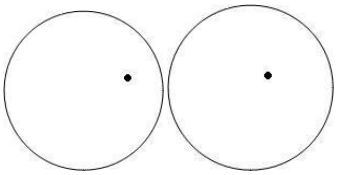

(c) View of a point in the mirrors

Figure 3.3 Two curved mirror with one camera model.

The results obtained from the vision system with metallic mirror shows the matching problem. The distortions of the images on both mirrors were different. For example, when a white checkered paper in both mirror images was examined, it can be easily seen that the distortion in the left mirror image of the paper and the distortion in the right mirror image were significantly different as shown in Figure 3.4. The reason of these differences of the distortion was that the distance between white checkered paper and center of the right mirror was more than the distance between the center of the left mirror as shown in Figure 3.3c. The matching problem caused from the different distortion of the white paper between the right and left mirror's images increased especially when looking from the right mirror's right side and has reached to a point where it was unresolved.

Figure 3.4 The image taken from the imaging system with two mirrors and a camera.

This matching problem may be overcome by developing calibration models for small ratios, but the developed model cannot be adequate for nonlinear and large scale distortions like in the Figure 3.4. While the calibration model is correcting the distorted areas, the undistorted areas in the image may be distorted by the calibration model. In addition, it was very hard to develop a nonlinear calibration model for this omni-directional imaging system. Therefore, imaging system with two curved mirrors and two cameras is chosen in the project for further studies.

3.1.2 Basic Imaging System with Two Mirrors and Two Cameras

The new imaging system was developed with two mirrors and two cameras. Besides, this system also included a Fiber Grating Device (FGD).

As shown in Figure 3.5, the vision system consists of two rectilinear mirrors aligned in a horizontal line with a distance D. Each of two CCD cameras with a refractive lens was fixed at a certain distance in front of the mirror.

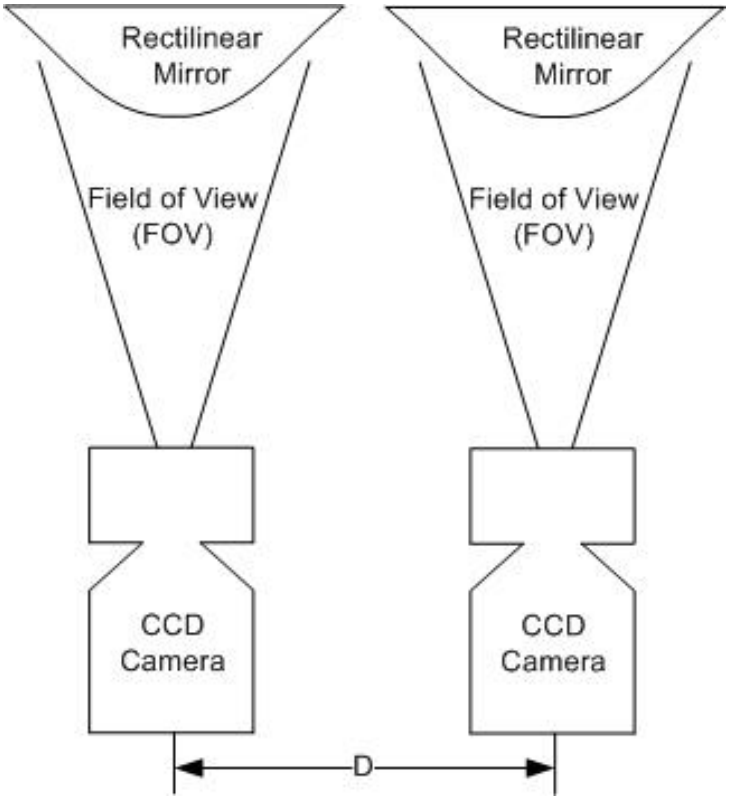

Figure 3.5 The vision system.

In the vision system, each mirror has 60mm radius circular base, 360^{o} FOV with horizontal axis and 151^{o} FOV with vertical axis as shown in Figure 3.6a. The required mathematical equations for calculating the reflection of the light from the mirror is also taken from the manufacturer.

Both of the CCD cameras have 410K pixel resolution and 1/3 inch CCD sensors (Figure 3.6d). The outputs of the cameras are analog, so a frame grabber device is used for converting the signal of the camera from analog to digital. Both cameras have holders (Figure 3.6c) and can be mounted with the mirrors as shown in Figure 3.6e.

Fiber Grating Device (FGD) consists of a green light laser beam with 30mW power and 532nm wavelength (Figure 3.6f), and a fiber grating for diffracting the laser beam into a dot-matrix pattern (Figure 3.6g).

The CCD cameras are placed outside of the focal points of the mirrors where the light beams intersect after the reflection from the mirror. To place the camera on the focal point of the mirror, a transparent plastic sphere cover is used (Figure 3.6b). Mirrors are put into the plastic cover and across the mirrors; camera and its lens are placed at the focal point of the mirror (Figure 3.6e). The focus of the camera is also adjusted with an adjustment mechanism over the transparent plastic sphere cover.

Both the imaging systems were mounted on a metal holder with 15cm distance to each other is given in Figure 3.7.

(a) Rectilinear mirror

(b) Transparent Plastic Cover

(c) Camera Holder

(d) CCD camera

(e) Mounted vision system

(f) Fiber Grating device

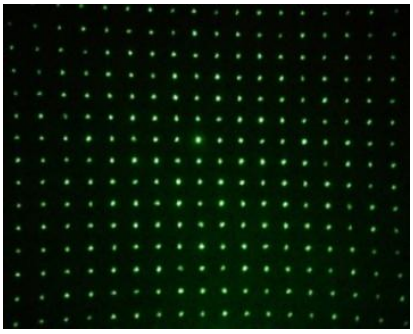

(g) Green light laser beam with matrix pattern

Figure 3.6 Hardware used in the project.

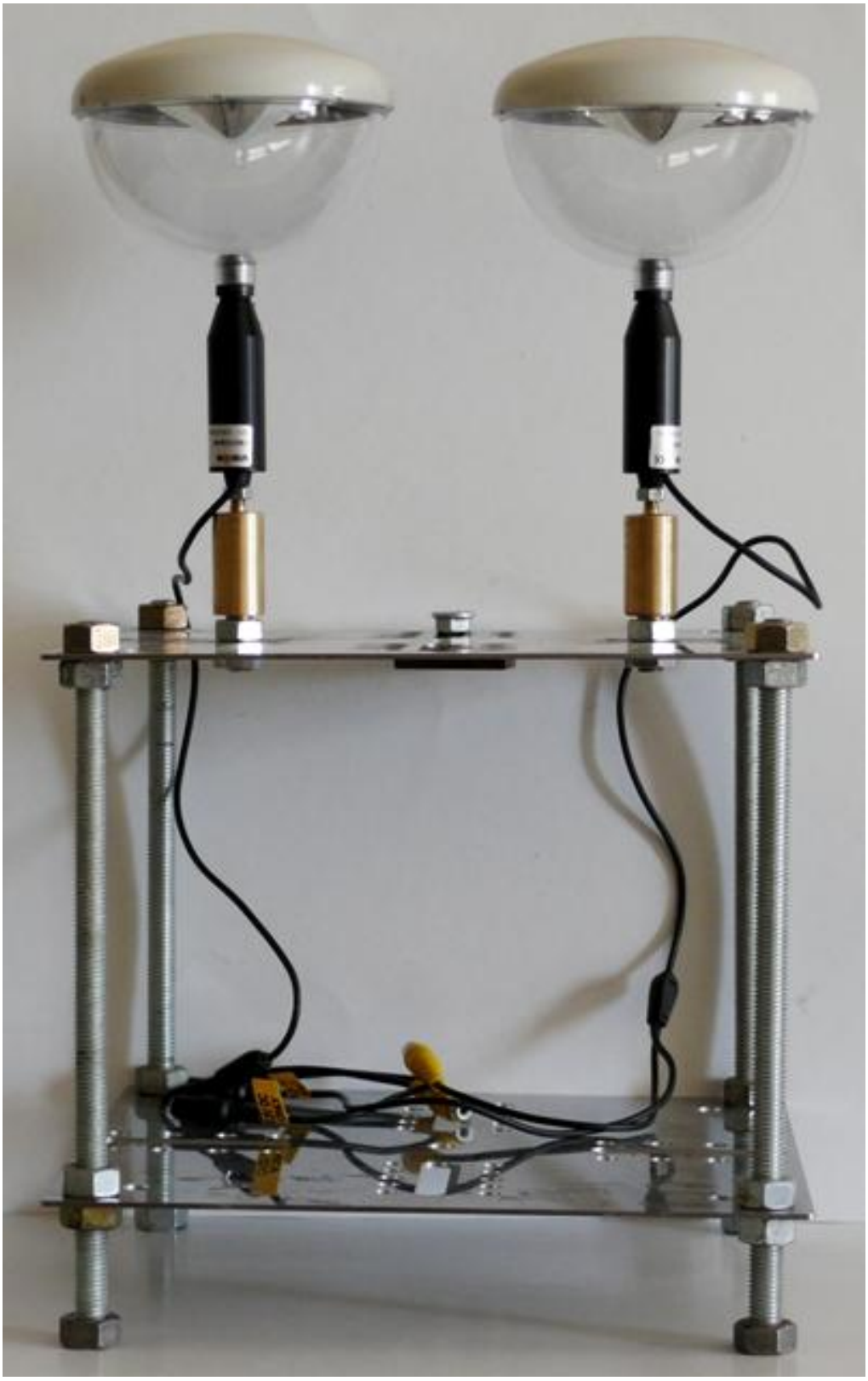

Figure 3.7 Imaging System mounted on a metal holder.

Vertical distance between focal point, which light beams intersection points after reflecting from the mirror, and the bottom of the center of the mirror is 42mm. The reflection of the light beams from the rectilinear mirror is given in Figure 3.8 (Kweon et al., 2006).

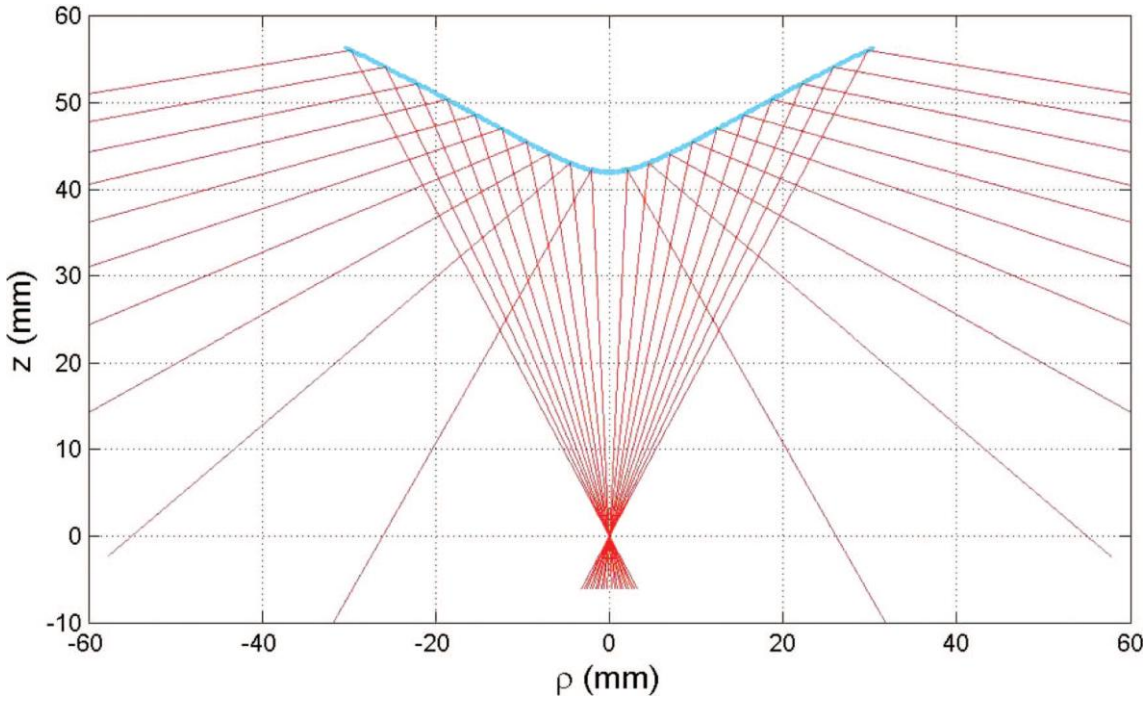

Figure 3.8 Reflection of the light from a rectilinear mirror (Kweon et al., 2006).

"*Due to the rectilinear projection scheme, the horizontal interval between the adjacent rays is nearly constant both before and after the reflection at the mirror.*" (Kweon et al., 2006). Therefore, the rectilinear mirror reflects a perspective image of the environment and the distance between the adjacent horizontal points in the projection image is nearly equal to each other. This property is called "*equidistance*".

To construct 3D structures of obstacles in the current environment and to find the distances of the obstacles from the vision system, a dot-matrix laser pattern is used as shown in Figure 3.9, This pattern is obtained by passing a laser source through a FGD and scattered in front of the environment of the vision system (Figure 3.10).

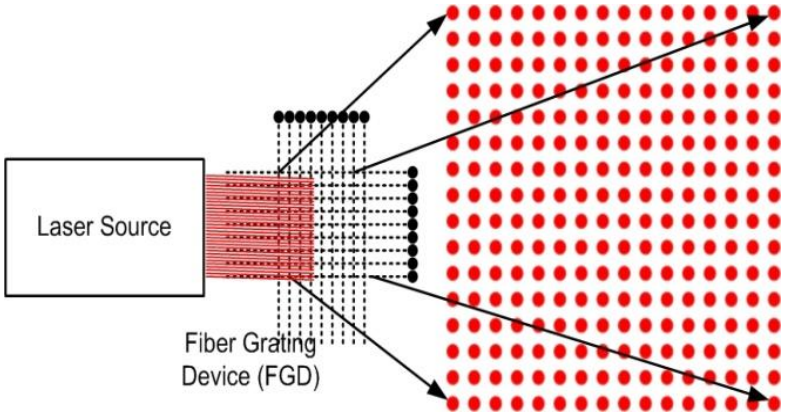

Figure 3.9 A dot-matrix laser pattern construction by using a laser source and a Fiber Grating Device.

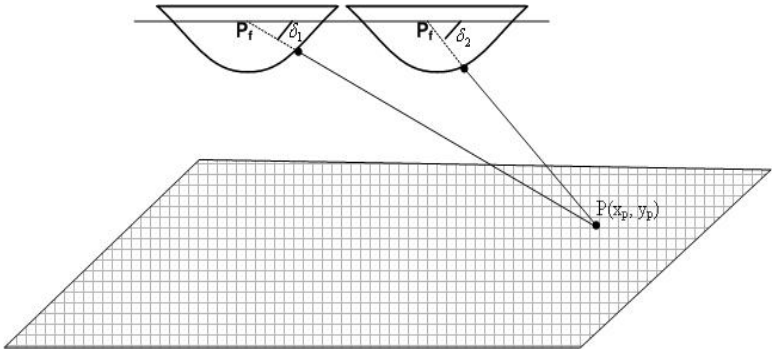

Figure 3.10 A dot-matrix laser pattern scattered on the environment of the vision system.

CHAPTER FOUR
SYSTEM SOFTWARE DEVELOPMENT

4.1 General Overview of the System

In order to identify obstacles in the environment different approaches may be applied. These approaches may be classified into two groups:

- Taking and processing images continuously.
- Taking and processing the image in a discrete timeline.

These kinds of imaging systems can be used to determine the obstacles in the environment. Generally the movement of the mobile robot is slow and the mobile robot is not always in a movement, so a discrete time approach method is more suitable for this application.

During the movement of the mobile robot, vision system will take two images from the environment by using this methodology. First image is simple environment image, and the second image is environment image with dot matrix laser spots. The obstacles which are placed in the environment can be determined by using these images. It is aimed that the vision system will process the images in a time short enough for safe mobile robot movement.

4.2 Determining Laser Points from 2D Images

4.2.1 Detecting Laser Points from Environment Images

In order to obtain an image of the environment by using laser spots, the prepared and adjusted vision system is used. Two images are taken from the environment. First environment image is taken before reflecting dot matrix laser spots to the area, and the second image is taken after reflecting dot matrix laser spots. All background images are eliminated except the laser spots by subtracting simple environment

image from environment image with dot matrix spots image. Both the simple environment image and environment image with dot matrix spots are given in the Figure 4.1. In this study, the image taken without laser points is called "*mask*" image (Figure 4.1a), the images taken with laser points is called "*live*" image (Figure 4.1b), and difference of these two images is called "*difference*" image (Figure 4.1c). *Difference* image converted to "*grayscale difference*" image as shown in Figure 4.1d.

(a) *Mask* image

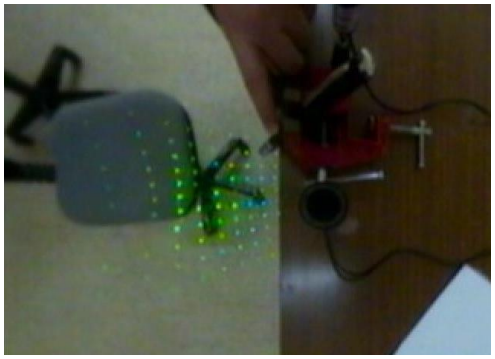

(b) *Live* image

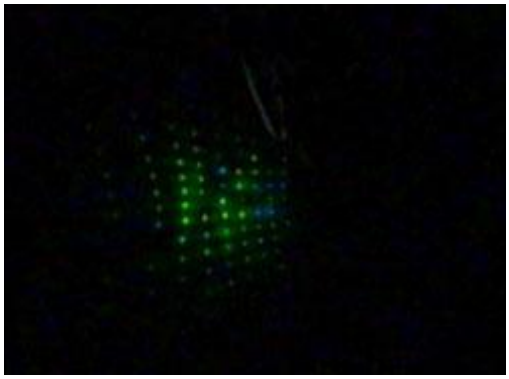

(c) *Difference* image

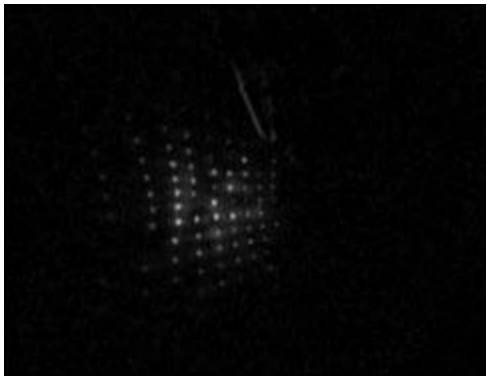

(d) *Grayscale difference* image

Figure 4.1 Detecting laser points from environment images.

A specific gray level is observed in the *grayscale difference* image caused by the reflections between the laser points. The real laser points in the environment need to be distinguished from the gray level points caused by the reflection. For this purpose:

- Smoothing operation is done by a 3x3 pixel neighborhood average value filter for each pixel in the *grayscale difference* image. After the operation Grayscale levels of the all pixels decrease a little. But, the gray levels, which are caused

by the reflection of laser spots, around the real laser spots are decreased, and these gray levels are not confused with the real lasers spots. The smoothed version of the image in Figure 4.1d is given in Figure 4.2a.

- After smoothing the *grayscale difference* image, a window size of 21x21 pixels is shifted by 21 pixel increment on the *difference* image then the average grayscale value is calculated for each window. This average value is multiplied with a constant number which is calculated by experimental studies on the grayscale images. After multiplication a threshold value is obtained. The pixels belong to the *Difference* image are eliminated if their grayscale values are under the threshold value, and they are set to 0, otherwise their values stay untouched. So that, the remaining noise after the subtraction process is recovered by this operation. Windows are shifted with 21 pixels range, so the overlapping consecutive windows are blocked and the algorithm is run faster. Recovered image is given in Figure 4.1b after recovery operation.

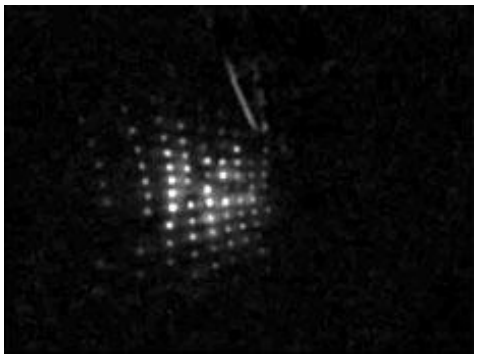

(a) Smoothed image

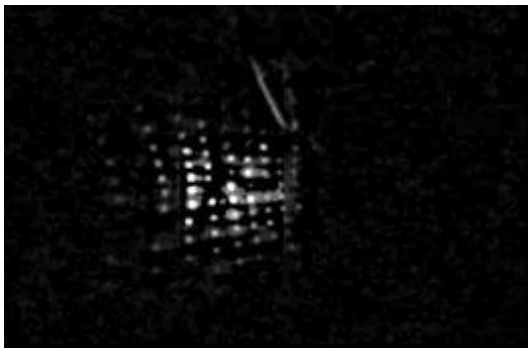

(b) Recovered image

Figure 4.2 Recovering laser images.

4.2.2 Determining General Positions of the Laser Points

Recovery operation over the laser points has been carried out by the elimination of the points whose grayscale values are under the determined threshold value in a particular ratio. Whereas, some reflection points over the threshold values are still remaining. In this situation, the expected purpose is not to find and eliminate these spoiled points, but to determine the common structure of the laser points on

grayscale *Difference* image after a particular smoothing and recovery operations to overcome the reflection problems. Thus, the center of the each proper laser point which is fitted with the common laser point structure can be determined by detecting the highest grayscale value of the each laser point as shown in Figure 4.3.

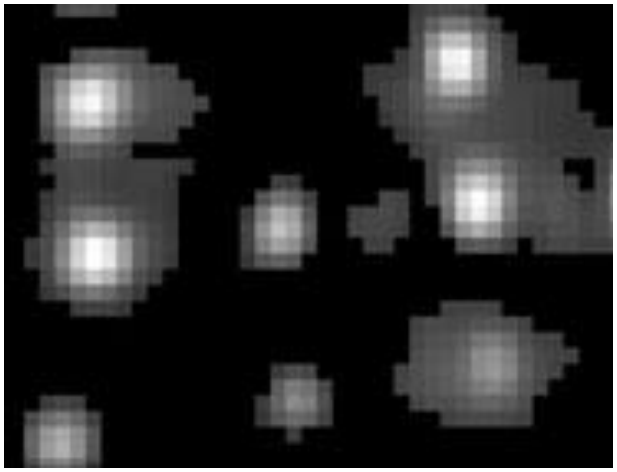

Figure 4.3 Zoomed Presentation of the recovered laser points.

4.2.3 Proper Laser Points and Circular Neighborhood

The position of a point in the environment can be determined only by comparing and finding the pixel's positions on the images taken from two different cameras. It was found that a laser point has a particular structure, and the brightest pixels were closed to each other. Therefore, it was also seen that the error ratio was decreased by using the brightest pixels positions when determining the real laser points place.

First important detail is the central pixels of the laser points have the highest gray level (brightest), and the gray level rate decreases when shifting the neighbor pixels in all directions. Another important detail is "*circular neighborhood*" structure. The group of the neighbor pixels in a window having the same brightness value are called *circular neighborhood* (Figure 4.4).

The model has four separate circular neighborhoods for each laser point. Circular neighborhoods from outer circle toward the center of laser points have 16 pixels, 12

pixels, 8 pixels and four pixels respectively. Recovered *difference* image's laser points should be found by considering this model.

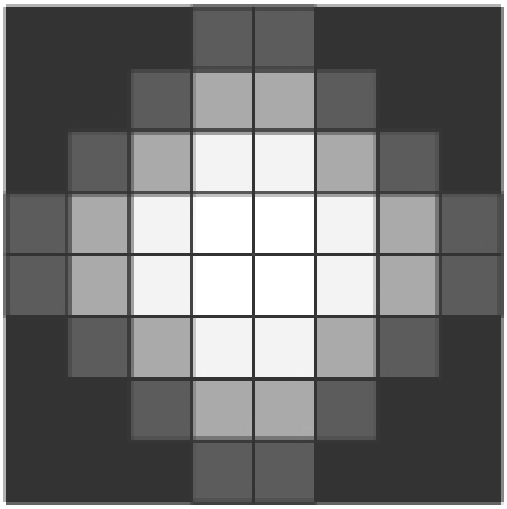

Figure 4.4 Circular neighborhood model.

4.2.4 Determination of the Laser Points Centers

The purpose of finding the center of the laser spots and determining center of the laser points, an algorithm is developed. In order to find the brightest point of the laser spot and to determine the real position of the laser point, an 8x8 pixels window is used. Four separate circular neighborhood model is based in this window. Similar to the operation for *Difference* Image, the circular neighborhood window, which is 8 pixels wide and 8 pixels height, is shifted one pixel in columns and then one pixel in rows.

Pixel in the upper left corner of the window is accepted as the beginning. The brightest point in the window is the innermost four pixels, which belong to a circular neighborhood, and is checked in each shifting progress.

The pseudo code of the determination of the center of the laser points algorithm is given in the next page.

```
Function Find_Center_of_the_Laser_Points(Parameters: Two dimensional array
form of the difference image)
      For each 8x8 pixels window size in the image array:
            Call Function Find_Biggest_Gray_Level(Parameters: all the
            pixel values in the 8x8 pixel window. Returns:
            The_biggest_gray_level in the 8x8 window)
            If The_biggest_gray_level < threshold value Then return 0
            Else
                  Calculate 16_pixel_CircularAverage from 16 pixel
                  circular neighborhood.
                  Calculate 12_pixel_CircularAverage from 12 pixel
                  circular neighborhood.
                  Calculate 8_pixel_CircularAverage from 8 pixel circular
                  neighborhood.
                  Calculate 4_pixel_CircularAverage from 4 pixel circular
                  neighborhood.
            End If
            If 12_pixel_CircularAverage - 16_pixel_CircularAverage <
            threshold value E1 Then return 0
            Else If 8_pixel_CircularAverage - 12_pixel_CircularAverage <
            threshold value E2 Then return 0
            Else If 4_pixel_CircularAverage - 8_pixel_CircularAverage <
            threshold value E3 Then return 0
            End If
            Calculate 12x12 pixel window average and assign to
            SquareAverage.
            Calculate average of the sum of the four circular
            neighborhoods and assign to CircularAverage.
            If CircularAverage – SquareAverage < threshold value E4 Then
            return 0
            Else
                  Set The_biggest_gray_level as center of the laser point.
            End If
      End For
Return Center of the laser points array.
```

In order to be sure that the window is placed on the bright laser spot region correctly and proper with the circular neighborhood model, additional controls should be carried out. An attention is given to the found brightest point if it is over a certain gray level. If the brightest spot is not in the 4x4 pixels window or under the threshold value, the window is shifted one pixel to the next position without any investigation. Thus, after this primary election the algorithms results more quickly, and considering same laser spots more than once was prevented.

If the average of 8x8 pixels window is over threshold value, and the brightest laser point is placed in (4x4) neighborhood, it is controlled that the window is set over a proper laser spot on the image. The brightness of the laser spot pixels should be increased toward to center of the laser spot when considering the circular neighborhood model on the recovered *difference* image. The arithmetic average gray level value of each circular neighborhood is calculated as in the circular

neighborhood model for this purpose. In this model from outside to the center 16, 12, 8 and 4 pixels average gray level values are calculated respectively. The difference between each calculated average pixel values are checked if they are grater or equal than E_1, E_2 and E_3 gray level threshold values.

$$(12\_pixel\_CircularAverage - 16\_pixel\_CircularAverage) \geq E_1$$
$$(8\_pixel\_CircularAverage - 12\_pixel\_CircularAverage) \geq E_2$$
$$(4\_pixel\_CircularAverage - 8\_pixel\_CircularAverage) \geq E_3$$

After the experiments, it was seen that when all of the threshold values are accepted to be equal to each other, this situation did not have a negative effect on determination of proper laser spots. If all of three equations given above are provided, this point is accepted as a laser point, and leads into the next stage of evaluation. In the second stage, the brightest points, which can be clearly distinguished from the other points (regions), selection process is carried out. This selection process enables to determine laser spots, and prevents to select wrong points between two laser spots caused by the reflection of spots on the image. Two distinct average values are calculated for this purpose.

`CircularAverage` value is calculated by adding all circular neighborhood averages and divided by 4. After that, `SquareAverage` value is calculated by taking average of 12x12 pixel new region after 2 pixel expansion of circular region. The difference between `CircularAverage` and `SquareAverage` is calculated. Then check the difference greater than E_4.

$$(CircularAverage - SquareAverage) \geq E_4$$

If the comparison result of E_1, E_2, E_3 and E_4 is positive then 8x8 window region called a “proper laser point”, and the brightest point placed in window (4x4) neighborhood is called “*laser point’s center*”. *Live* image with laser spots and laser point’s centers image after determining center pixels are given in Figure 4.5.

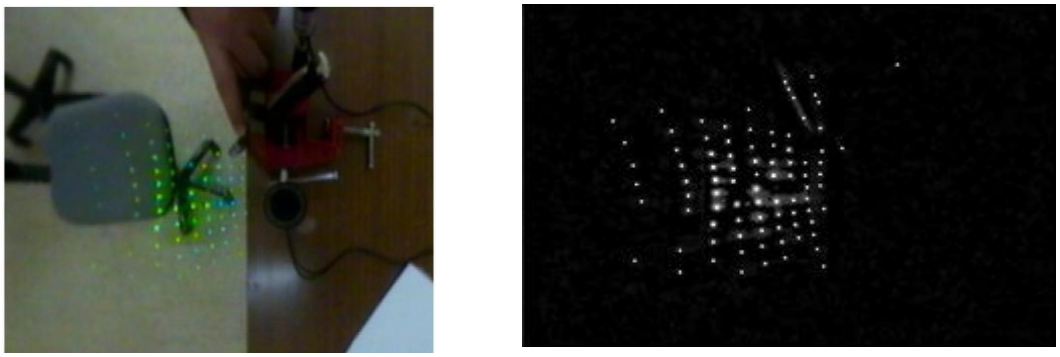

(a) Live image (b) Center of the laser points

Figure 4.5 Laser point's centers image after determining center pixels.

During the implementation of the system, the laser light source is being switched by hand, so the scattered laser spots in the image are formed. This problem will be overcome after the laser light source is mounted on a stable platform and switched by an electronic control system.

4.3 Obtaining 3D Positions of the Laser Points

After the center of an image (x_m, y_m) is accepted, x is represented by the horizontal position and y is represented by the vertical position in a two-dimensional image. $p_1(x_{p1}, y_{p1})$ is the point in the first image captured by the first camera-mirror pair and $p_2(x_{p2}, y_{p2})$ is the point in the second image captured by the second camera-mirror pair placed at a distance, L from the first camera-mirror pair as shown in Figure 4.6. L is the vertical distance between two imaging systems. The coordinate axes of both systems should be in parallel with each other.

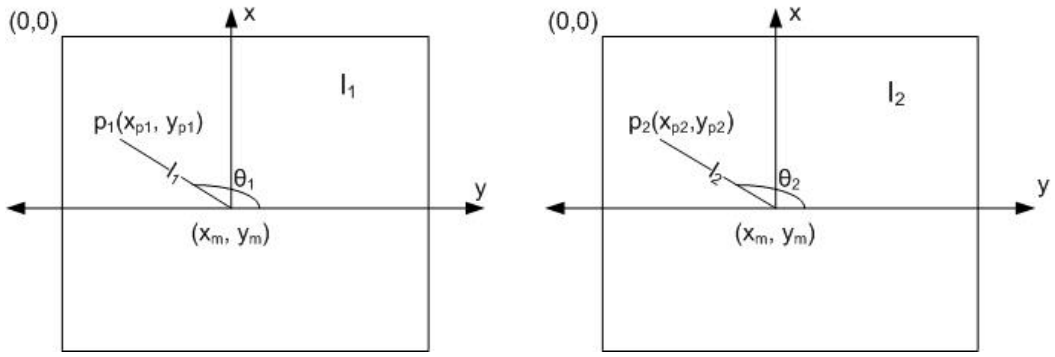

a) Point p_1 on the I_1 image and its distance l_1 from the center of the image.

b) Point p_2 on the I_2 image and its distance l_2 from the center of the image.

Figure 4.6 Projection drawing of a point on both image planes.

By using the formula between two points in particular coordinates the Equation (1) and (2) can be formed:

$$l_1 = \sqrt{(x_m - x_{p1})^2 + (y_m - y_{p1})^2}\,\frac{D}{d} \qquad (1)$$

$$l_2 = \sqrt{(x_m - x_{p2})^2 + (y_m - y_{p2})^2}\,\frac{D}{d} \qquad (2)$$

D is the real curved mirror base circle diameter, and *d* is the diameter of the curved mirror's base on the image of the mirror. Since all of the coordinate values of points are measured on the image, it is necessary to convert these lengths to pixel or distance format in millimeter before calculating the distance. The angles, which is formed by the lines, which join the points whose row and column values are known, with the *Y-axis* are calculated from Equations (3) and (4).

$$\theta_1 = \tan^{-1}(\frac{\Delta x}{\Delta y}) = \tan^{-1}(\frac{x_m - x_{p1}}{y_m - y_{p1}}) \qquad (3)$$

$$\theta_2 = \tan^{-1}(\frac{\Delta x}{\Delta y}) = \tan^{-1}(\frac{x_m - x_{p2}}{y_m - y_{p2}}) \qquad (4)$$

θ_1 and θ_2 angles are used to determine *x* and *y* coordinates of a point in the environment on the horizontal plane. In order to calculate height value *Z* of a point perpendicular to the *XY* plane, the light's angel of reflection from the mirror should be used. The angle between the reflected light ray from the mirror and the vertical

axis through the center of the mirror is called α angle as shown in the Figure 4.7 (Kweon et al., 2006). This reflected light ray from the mirror forming the angle, the vertical axis through the center of the mirror and the line combining the reflected light ray point on the mirror and center of the vertical mirror axis forms a triangle as shown in Figure 4.7. Not only the calculated the l_1 and l_2 values for each images are the perpendicular edges of the triangle, but also correspond to a radius on the mirror for that point.

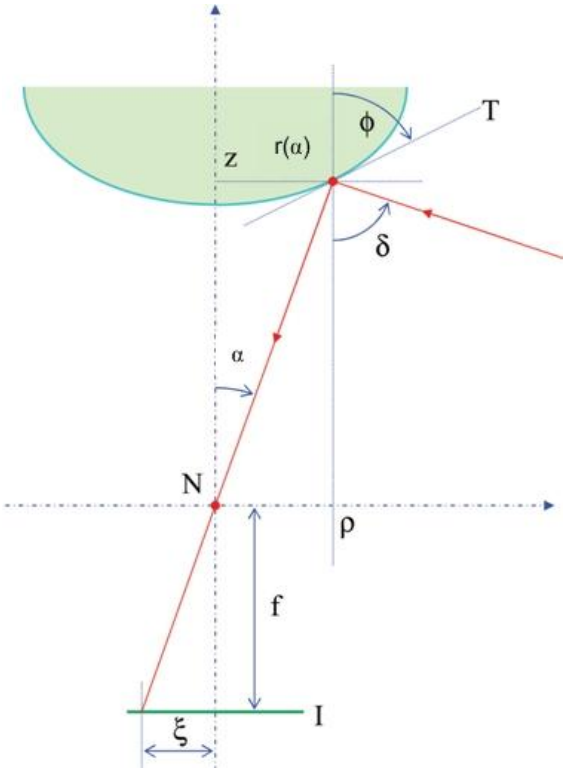

Figure 4.7 Reflection of a light ray from the environment on the rectilinear mirror as shown with a red line (Kweon et al., 2006).

By setting out equality from opposite angles, the image sensor length ξ, focal length (f) on the camera and the light reflected from the surface of the mirror in the opposite direction is formed a right triangle. Here, between the ξ length and α angle a correlation is found (Kweon et al., 2006).

$$\xi = f \tan(\alpha) \qquad (5)$$

The f value of the camera's focal length is known. The correlation between δ angle, depending on the α angle, created by the light from the environment and α angle is given (Kweon et al., 2006).

$$\delta(\alpha) = \tan^{-1}(\frac{\tan\delta_r}{\tan\alpha_r}\tan\alpha) \qquad (6)$$

The value of α_r angle on the right hand side of the Equation (6) is the angle that the curved mirror can view the corner of the image with a 4:3 ratio (640x480 pixels) after it's assembled to its sphere and adjusted for focus.

This value is equal to α_r=26.565^o in the purchased mirror, and the corresponding border angle is δ_r=*80*° (Kweon et al., 2006). By using Equation (6);

$$\frac{\tan(\delta(\alpha))}{\tan\alpha} = \frac{\tan\delta_r}{\tan\alpha_r} = 0.08816$$

Ratio can be calculated (Kweon et al., 2006). There is such an equation between α and δ angle equals to a fixed number in the existing rectilinear mirrors (Kweon et al., 2006).

The ξ length can be calculated by using calculated *l* length value from the image system, and then α angle can be calculated by putting ξ length in equation (5). After calculating α angle value, δ angle the light ray coming angle is obtained from equation (6). This angle gives the direction of a point, which is representing a real point in the visible environment, in the image. When the position of a point placed in the environment in the horizontal image plane (*real X and Y coordinates*) is founded, this point's vertical coordinate (*Z height value*) can be easily found by using δ angle value between the light ray direction reaching the curved mirror from this point and vertical axis.

An image and an equivalent p*(x, y)* values in the vertical image plane of a point in the environment are represented in Figure 4.8.

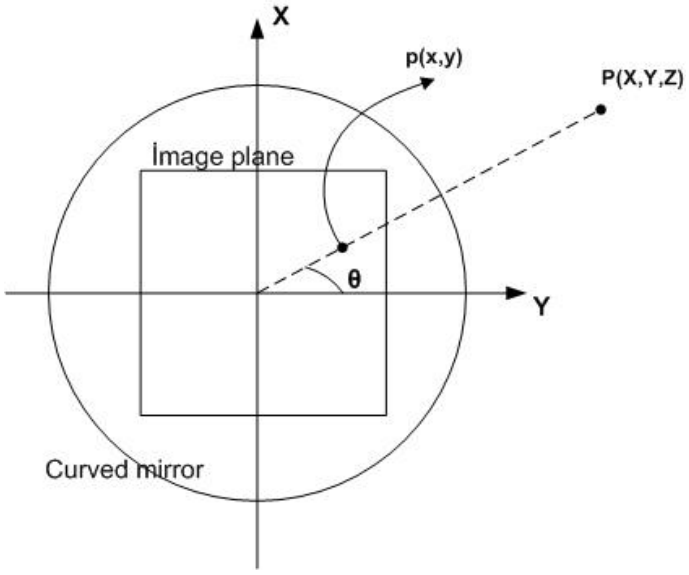

Figure 4.8 Horizontal view of mirror and image plane.

By using this relation in Figure 4.8, the following equation (7) can be written.

$$\tan\theta = \frac{X}{Y} = \frac{x}{y} \qquad (7)$$

To determine the horizontal position of a point in the environment (real X, *Y* coordinates) six different regions should be taken into account as shown in Figure 4.9. When calculating the vertical distance of the points in the environment from the imaging system, this point's position is becoming important against the both camera-mirror pairs placed in the imaging system with an *L* distance to each other. For example, calculated equations of a point placed in the III. Region for two camera-mirror system pair:

$$\tan\theta_1 = \frac{A}{\Delta Y_1} \text{ , } \tan\theta_2 = \frac{A}{\Delta Y_2} \text{ .}$$

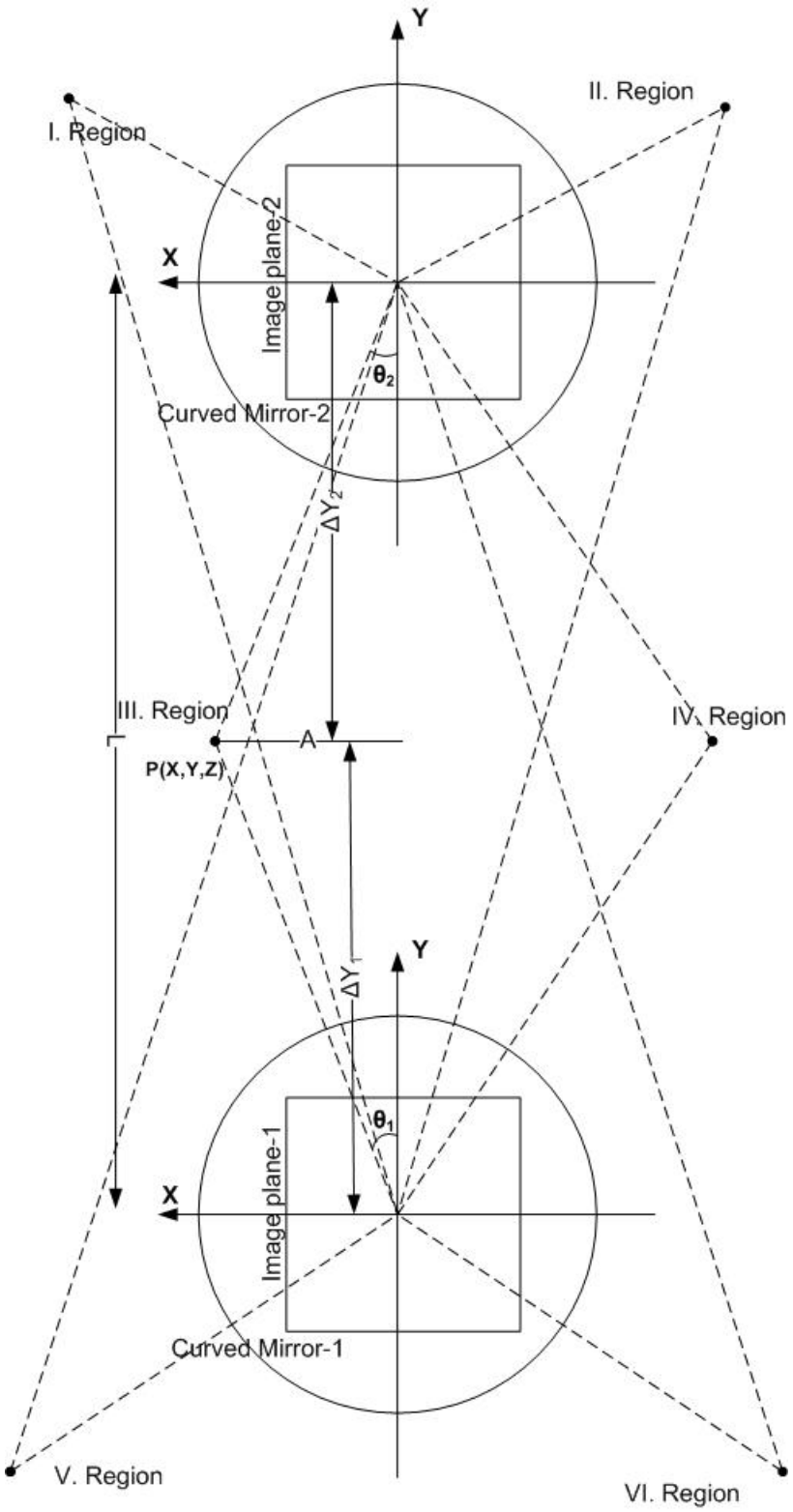

Figure 4.9 All of the possible positions of a point according to the imaging system.

The variable *A* is same for these two equations. Thus, Equation (8) below can be written;

$$\Delta Y_1 \tan\theta_1 = (L - \Delta Y_1)\tan\theta_2 \qquad (8)$$

Here, $tan(\theta_1)$, $tan(\theta_2)$ and *L* values are known. So that, ΔY_1, *A* and ΔY_2 values can be calculated from equation (8). Actually, Value *A* is equal to *X* of the *P(X, Y, Z)* as shown in the Figure 4.9. Moreover, value *Y* of this point can be calculated because θ angle value is also known. The horizontal distance of a point which *X* and *Y* real values are known from the imaging system, can be calculated with Equation (9).

$$L_{X-Y} = \sqrt{X^2 + Y^2} \qquad (9)$$

The 3D distance of this point from the imaging system can be calculated with the Equation (10).

$$L_{X-Y-Z} = \frac{\sqrt{X^2 + Y^2}}{\sin\delta} \qquad (10)$$

Z value can be obtained from calculating 3D positions of *P(X, Y, Z)* point by using the equations above.

4.4 Calculation of Positions, Errors and Calibration

4.4.1 Formation and Causes of Errors

There may be some mechanical errors that can occur on mirrors, cameras, lenses and other equipment during the production progress or when they are worked together. These errors are caused by unmatched x and y coordinates on both image planes during the assembly process, resolution problems during the production of cameras or some distortion problems on the image. Sometimes, elimination of these errors can be obtained by some mechanical adjustments, but in general these errors can be recovered by software solutions. This process is called "*calibration*".

An omni-directional vision system consists of mirrors, cameras, lenses and the platform where they are put together. There are some different approaches to eliminate errors caused by the components.

In the first approach, a classic camera with a narrow FOV is calibrated alone. After that the camera is mounted into the imaging system, and the whole imaging system is calibrated again.

In another approach, all the mirrors and camera systems are calibrated as a whole. While calibrating the camera alone, especially the camera's internal and external parameters must be known. However, it is not needed to use these parameters when calibrating the integrated systems.

The cameras included in our project can be used only with special refractive lenses produced for rectilinear mirrors. These cameras and lenses should be used together.

The cameras used in this project cannot be used with classical lenses because the measured distance between two points for equal height from the floor cannot be changed by the camera and vision system distance, so a consistent distance measurement cannot be done with general lenses.

Refractive lenses used in the vision system reflect the light toward to camera’s image sensor, and forming an understandable image on the camera. Moreover, the distance between the adjacent horizontal points in the projection image is nearly equal (equidistance) to each other. Especially, the presences of these lenses are used in imaging systems don’t need to use classic methods, for example, checkerboard pattern using a camera-lens calibration standards (Zhang, 2000).

Using the matched points obtained from two separate images by using two mirrors and two cameras, the real *X, Y, Z* coordinate values of these points can be calculated. However, sometimes, the camera-mirror pairs are not located in the same *x, y* axes

physically and the mechanical differences in the camera and mirrors can cause some errors when matching the laser points in the developed vision system. Moreover, these matching problems may cause other errors in further calculations.

In this study, in order to overall vision system calibration purposes and eliminate errors in the images, a mathematical based calibration methodology is developed for the stereo vision system which is fixed on vertical axis with a certain height from the floor.

4.4.2 Matching Laser Points in an Environment with no Obstacle

The level of successful calibration of imaging system is based on the matching success of the center of the laser points in the imaging system. The reason for this is the difference between the point's location in two matched images while calculating the distance of a point from the system and its height from the floor in the real world. Therefore, in order to match the pixels in the image taken from the first camera with the pixels taken from the second camera, calibration should be performed.

The *X-axis* of the imaging system that represents the rows in the image, is in the same direction with the *Y-axis* of the imaging system which represents the columns. The mechanical parts of two mirror-camera combination in the imaging system are mounted in the same direction on the *X-axis* with a 150mm distance between them and facing each other on the *Y-axis* as shown in Figure 4.10.

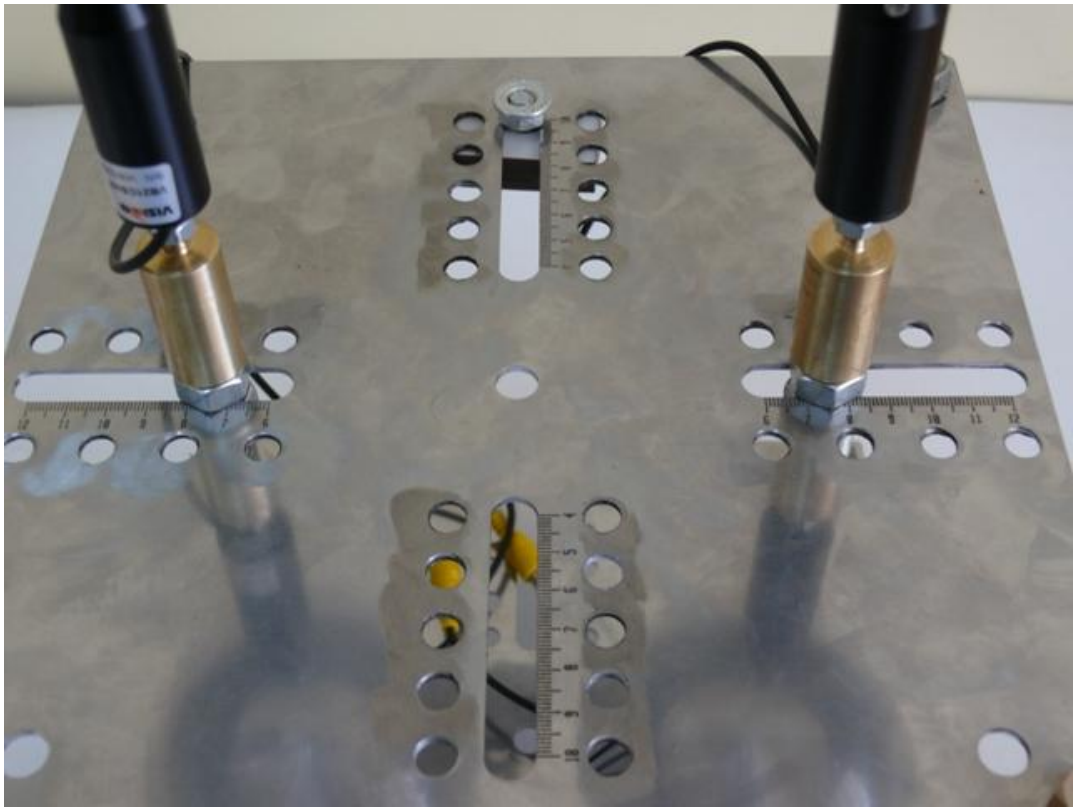

Figure 4.10 Alignment of the vision system.

When the images taken from the cameras are considered matrices created by pixels, row values are accepted horizontal axis and column values are accepted vertical axis. First and fourth degree two polynomials are used for constructing the mathematical model. The row value of the center of the laser point in the main image is converted to the row value of the center of the laser point in the matched image by using first-degree polynomial because these points are in the same direction. Then, The column value of the center of the laser point in the image is converted to the column value of the center of the laser point in the matched image by using fourth-degree polynomial because they are not in the same direction and matching the column values are more complicated. The pseudo code of the matching algorithm is given in the next page.

```
Function Matching_the_Laser_Points(Parameters: two dimensional arrays of two
images taken from the left and right side cameras of the vision system)
       Set the array of the left side image as image 1, and the array of the
       right side image as image 2.
       Get polynomial coefficients matrix Xr for rows, and polynomial
       coefficients matrix Xc for columns.
       For each center of the laser points in image 1:
              Set the region value of searching for matching N to 1.
              Calculate the row and column values of the possible position
              of the laser point in image 2 with multiplying the row and
              column values of the laser point in image 1 by Xr and Xc
              polynomial coefficients matrices, respectively.
              For each laser point with N neighborhood in image 2:
                     If The gray level of the calculated position of the
                     laser point in image 2 is smaller than 255 gray level.
                     Then
                            Add the unmatched laser point row and column
                            values in the unmatched laser points list.
                            Increase the unmatched laser point count by one.
                     Else
                            Set the calculated position of the laser point in
                            image 2 as a matched laser point with the laser
                            point in image 1.
                     End If
              End For
       End For
       For each unmatched laser point in the unmatched laser point list:
              Update Xc polynomial coefficient value by subtracting a margin
              value in order to find a matched laser point in image 2.
              Margin value is used for to match laser points above the
              ground level.
              Calculate the row and column values of the possible positions
              of the laser point in image 2 with multiplying the row and
              column values of the laser points in image 1 by Xr and Xc
              polynomial coefficients matrices, respectively.
              For each laser point with N neighborhood in image 2:
                     If The gray level of the calculated position of the
                     laser point in image 2 is smaller than 255 gray level.
                     Then return 0
                     Else
                            Set the calculated position of the laser point in
                            image 2 as a matched laser point with the laser
                            point in image 1.
                     End If
              End For
       End For
Return Matched laser points two dimensional image array.
```

Images are captured from each camera, and the centers of the laser points are determined, and in order to match rows Equation (11) is used:

$$y_r = l_1 r + l_2 \tag{11}$$

And to match columns Equation (12) is used:

$$y_c = k_1 r^3 + k_2 c^3 + k_3 r^2 c^2 + k_4 r^2 c + k_5 r c^2 + k_6 r^2 + k_7 c^2 + k_8 r c + k_9 r + k_{10} c + k_{11} \tag{12}$$

Here, r is the row value and c is the column value of a pixel in the first image. y_r calculated from Equation (11), gives the first image's equivalent row value on the second image, and y_c calculated from Equation (12), gives the first image's equivalent column value on the second image.

For calculating l and k coefficients Least Squares method is used. So the Equations (11) and (12) can be written as Equations (13) and (14);

$$Y_r = A_r X_r \tag{13}$$

$$Y_c = A_c X_c \tag{14}$$

Definitions of the matrices in Equation (13) and (14) are given below;

$A_r = [r \;\; 1]$

$X_r = [l_1 \;\; l_2]$

$Y_r = [y_{1r} \;\; y_{2r} \;\; . \;\; . \;\; y_{nr}]$

$A_c = [r^3 \;\; c^3 \;\; r^2c^2 \;\; r^2c \;\; rc^2 \;\; r^2 \;\; c^2 \;\; rc \;\; r \;\; c \;\; 1]$

$X_c = [k_1 \;\; k_2 \;\; k_3 \;\; k_4 \;\; k_5 \;\; k_6 \;\; k_7 \;\; k_8 \;\; k_9 \;\; k_{10} \;\; k_{11}]^T$

$Y_c = [y_{1c} \;\; y_{2c} \;\; . \;\; . \;\; y_{nc}]$

To solve the Equations (13) and (14) in the form of a linear matrix, first, A_c and A_r matrices with Y_r and Y_c solution vector must be created. Sufficient number of row r and column c values of matrix A, and the equivalent y_r row and y_c column values of these pixels in the second image should be known. These points are called "*control points (pairs)*" for the calibration process.

After selecting the control points determined in the vision system, the matching process is done manually and determined the coordinates for each point in two camera images. Then, A_r and A_c matrices are calculated by using these coordinates. In order to calculate the coordinates of any point along the horizontal axis the matrix A_r is used. Similarly, to calculate the coordinates of any point along the vertical axis the matrix A_c is used. X_c and X_r coefficients are obtained by solving ($Y=AX$) equations. The matched row and column values of a point of ,which row and column

points in the first image is known, can be calculated in the second image by using coefficients in the Equation (11) and (12).

For matching laser spots, the center of laser point's row and column values are put into place in Equation (11) and (12), and then the matched row and column values of that point in the second image are calculated. The purpose of controlling, pixel of this value is investigated with two pixels neighborhood whether a laser spot belongs on the second image. If there is a laser spot discovered in this neighborhood, points on the two images are matched with each other. All pixel pairs matched at this stage are used as control pairs for a secondary control stage.

In the secondary control stage, the control pairs founded in the first stage are used for calculating the X_c and X_r coefficients again. All transactions performed for the first stage are calculated again in the second stage with a neighborhood of one pixel. At the end of this stage X_c and X_r coefficient values are calculated again by using the pixel row and column values and the calibration process is ended.

At the end of a three-step calibration process, coefficients are used for calculating the length and height values of objects in the environment, and calibrated angle values of the vision system are obtained.

4.4.3 Matching Laser points in an Environment with Obstacles.

First of all, the center of the laser points for each image is determined in the environment having obstacles. After the center of laser point's row and column values are determined, they are put into place in Equation (11) and (12) and then the matched row and column values of that point in the second image are calculated. However, adding an experimentally calculated integer value *n (n= 1, 2, 3, ..., m)* to Equation (12), Equation 18 is obtained.

$$y_c = k_1 r^3 + k_2 c^3 + k_3 r^2 c^2 + k_4 r^2 c + k_5 r c^2 + k_6 r^2 + k_7 c^2 + k_8 r c + k_9 r + k_{10} c + k_{11} - n \quad (18)$$

Here *n* is only used for matching process after the results obtained from the experiments about hardware resolution of the imaging system. It is observed that, each increment of this number corresponds to an increase of 15cm in the image of the environment. This value is constantly increasing during the matching process, until a matched point is found at that phase. When a matched point is found, that point will be removed from the matching point set, then n value is increased by one and matching process continues. However, the heights of the points are not calculated by using this value, they are depending on the other parameters used to calculate distance and height.

For example; when a matching is done for *n=0,* the center of the matched points are at the ground level in the real world, for the matching *n=1,* the center of the matched points are above the ground level, the laser beam hits to an obstacle and there is an obstacle at that point.

The height of the laser point varies depending on the location of obstacles. Laser points are closer to the vision system when they are over an obstacle. Different height and length equivalents over the vision system pixels are also different. While the obstacle is getting higher, pixel values of the laser spots are shifting over the column more than the row on the first and second images. Therefore, the polynomial will be used to match column values should be changed the column value depending on the height, more. Otherwise the matched point on the second image could not be obtained.

Although the implementation of this process is a little more complicated, for *n=0* value, all the matched points are at the ground level, so these areas are available for travelling the mobile robot carrying the vision system.

During the matching process the unmatched points are accepted "*noise*" and these points are removed from both of the images. However, some real points are also removed from the both images because both cameras have different FOV. Therefore,

some points detected in the first image cannot be determined in the second image and these unmatched points are also accepted as "*noise*" and removed from the images.

At the end of the matching process, the distance in the horizontal plane and height value in the vertical axis are calculated according to vision system by using the θ_1, θ_2 and δ angle values calculated before from the calibrated two images. Calculated θ_1, θ_2 and δ angle values used for the calibration process are not required to be recalculated unless the physical structure changed.

4.4.4 Calculation of Distance and Height

In order to minimize errors in calculating the distances, the vision system is calibrated with two images of a horizontal plane with no obstacles. For this purpose, the imaging system positioned to a certain height from the ground. A matrix laser pattern is given to the environment with a fiber grating laser device placed in the middle of two camera-mirror pairs. Since there is no obstacle in the environment, all lasers spots are spread to the floor and all have the same height according to the vision system.

Calculation of distance and height of operations are started by using the image taken from a single camera first. After that, matching is done by using the image taken from the second camera, and the angular positions of the all laser points in the images are determined by using the results of the both matched images.

The pseudo code of the calculation of the 3D positions of the laser points algorithm is given in the next page.

```
Function Calculating_3D_Positions_of_the_Laser_Points (Parameters: row and
column values of center of a matched laser point in the first image, row and
column values of center of a matched laser point in the second image, teta1
angle which is the angle between the laser point and the center of the
horizontal image plane of the first image, teta2 angle which is the angle
between the laser point and the center of the horizontal image plane of the
second image, delta angle which is the angle between the center of the
vertical axis and the center of the laser point in the first image)
      For each matched laser point pairs in both images:
            Get r_ref row and c_ref column values, and X_ref and Y_ref real
            distances of the reference point.
            Get height of the vision system from the floor and assign to
            h.
            Get the real world equivalent Rr row and Rc column distances
            corresponds to one pixel.
            Calculate a real pixel horizontal X and vertical Y distances
            in the first image by using the teta1 and teta2 angle values.
            Calculate the Z vertical distance value by using delta angle.
            Calculate horizontal distance of the laser point from the
            center of the image plane and assign to Lxy.
            Calculate the real distance of the laser point from the first
            camera and assign to Lxyz.
      End For
Return the calculated X, Y, Z, Lxy horizontal distance and Lxyz real
distance values.
```

Due to the characteristics of the calibration process, a certain distance from the ground-level to the imaging system corresponds to the number of previously calculated pixels. Equidistance property of the mirrors is used to calculate the distance between two laser points. By the logical meaning of the equidistance property, the distance of a pixel at the ground level is the same everywhere in the environment. Starting out from this point, the vertical distance of a one pixel in the first image is known in the real world, the real *X* and *Y* positions of that pixel; all the other pixel's real world distances from the vision system can be calculated.

This calculation can be written as Equation (15) and (16):

$$X = X_{ref} + R_r(r - r_{ref}) \tag{15}$$

$$Y = Y_{ref} + R_c(c - c_{ref}) \tag{16}$$

Where;

r_{ref} , c_{ref} : The reference pixel's row and column values on the first image.

X_{ref} , Y_{ref} : The reference pixel's real horizontal and vertical distances from the vision system.

r , c **:** The pixel's row and column values of an equivalent point in the real world which will be calculated on the first image.

R_r , R_c, **:** One pixel's equivalent area size in the real world.

Also, for each imaging system, θ_{irc} angle values are calculated for each pixel on the images. Here, *i* shows the imaging system, *r* refers to row and *c* refers to column values.

R_r and R_c values may vary with respect to the resolution of the image and the distance of an object from the image plane. A pixel in the image corresponds to large area in low resolution and small area in high resolution. In this case, the horizontal and vertical dimensions of the area are also changing. Moreover, although there is no change in the resolution when the vision system getting further, the area shown in one pixel is getting larger and the sensitivity of the vision system is decreased. For example, the R_r value of one pixel is equal to 10.80 mm when the vision system is mounted 1,170 mm height from the floor.

The equivalent pixels of each pixel in the first image with the second image are calculated by using matching algorithm. In the case of an existing obstacle in the environment, the center of a laser spot's position is placed over or near the obstacle, vertical height and/or horizontal distance will be different from the other points. In addition, the images taken from the both cameras belonging to that point will bring different angular values and different coordinates (Figure 4.11). In this case, to determine the location of that point, θ_{irc} angle values which are calculated before, are used.

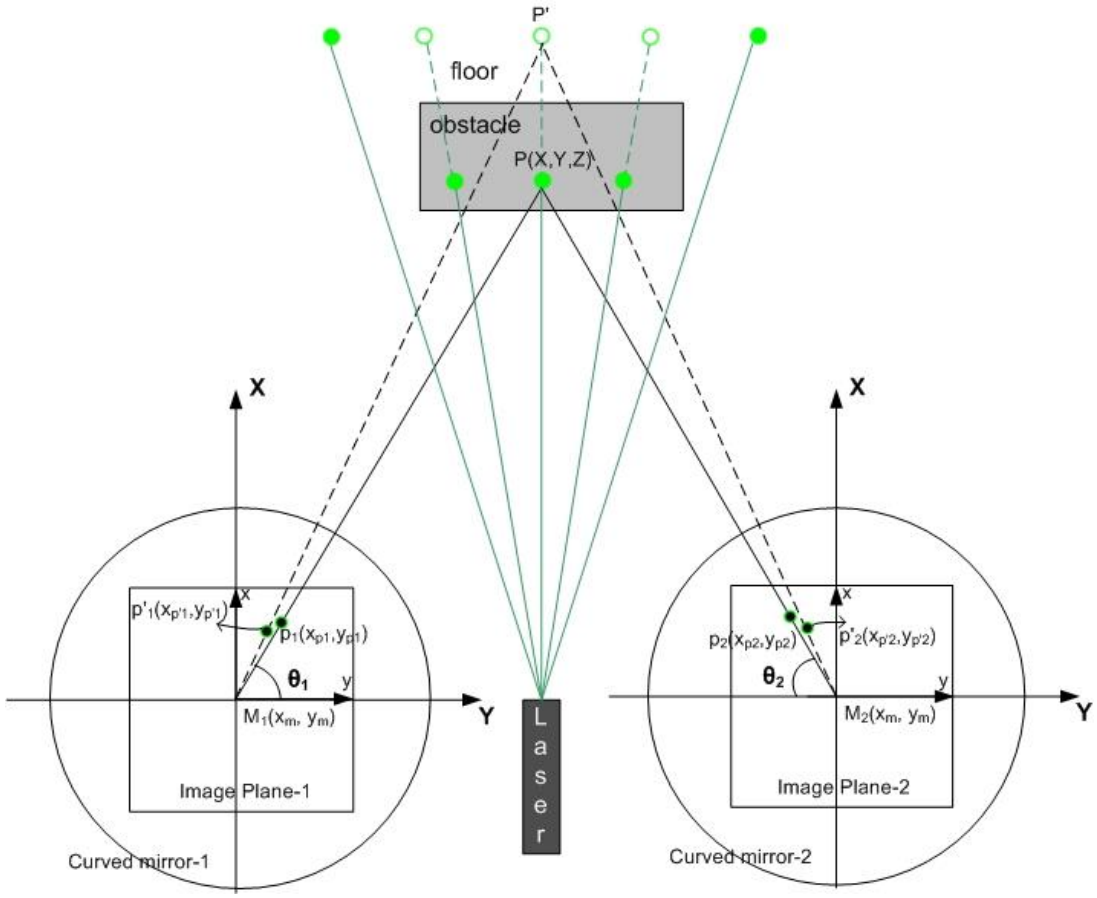

Figure 4.11 Horizontal plane distances and angular relationships of stereo imaging.

Here;

P: Real Point.

P′: The point of the laser ray will go in environment with no obstacle.

p_1, p_2: The projection of the real point on both mirrors.

p_1', p_2': *P′* point's projection on both mirrors.

θ_1, θ_2: The angle between the line passings thought the P point and the image plane.

M_1, M_2: center of the mirrors.

According to the shape of obstacles, when the location of the laser spot is changed in the horizontal plane, the location of the laser spot on the both images may be also changed. When new positions are taking into account, the location of a laser point

over an obstacle will be determined by using θ_1 and θ_2 angle values corresponded to the row and column values on both images, by using Equations (7), (8) and (9).

In order to calculate height of a laser point, horizontal distance and height from the horizontal plane of the imaging system is used. δ angle value calculated by using this value in Equation (17) is used in the Equation (10) and height of the laser point *Z* is calculated.

$$\delta = \tan^{-1}\left(\frac{\sqrt{X^2 + Y^2}}{h}\right) \tag{17}$$

Here, value *h*, is used to describe the height of the vision system from the ground.

The height values of objects in the real world will be the same for both the imaging systems; only to find δ values in the first image of the pixels is sufficient.

Since the row and column values of the pixels obtained from the both imaging systems are integers, during the matching process the results obtained from mathematical equations are rounded to integer values. For this reason, the same row and column values of the pixels could not be determined exactly. Moreover, the error rate of the polynomials using for calculating coefficients is raising near the images boundaries. For these reasons, there are some problems encountered when matching the two images each other.

In the case of finding unmatched pixels, first images is taken as a reference, and if there is a not matched pixel found in the second image, this pixel's angel value and location is determined by taking the arithmetic average of the pixels placed around that pixel.

The pseudo code of the rectilinear calibration algorithm is given in the next page.

```
Function Rectilinear_Calibration(Parameters: reference points set
Matching_Set1 from image 1, reference points set Matching_Set2 from image 2)
      Set the region value of searching for matching (calibration level) N
      to 2.
      Create row polynomial coefficients matrix Xr, and column coefficients
      matrix Xc.
      Create the polynomial variables matrix for row values Ar and for
      column values Ac.
      For calibration level N equal 2 down to 1 Do
            Set first column of Matching_set2 as matched row values Yr,
            and second column of Matching_set2 as matched column values
            Yr.
            Calculate Xr and Xc polynomial coefficients matrices from the
            solution of the equation Y=A*X. This equation can be written
            for row values Yr=Ar*Xr and for column values Yc=Ac*Xc.
            Call Function Matching_the_Laser_Points(Parameters: two
            dimensional arrays of two images. Returns: the Matched Laser
            point's image array)This function is used for matching the
            laser points with no obstacle then creating the new Matching
            Sets for the next calibration level.
            Create the new Matching Sets from matched laser points after
            matching the laser points.
      End For
      Get the teta1, teta2 and delta angle values matrices for the image 1
      for 3D distance calculation of the real positions of the laser points
      later.
Return Xr, Xc polynomial coefficients, and teta1 teta2 and delta angle
values matrices.
```

4.4.5 Developed Software for the Project

At the beginning of the project MATLAB is used. During the MATLAB usage, algorithms are improved, images are obtained and errors in the algorithms are fixed more quickly.

After all system was developed, algorithms developed by using MATLAB also implemented into C#.NET language for the purpose of controlling the mechanical systems of the mobile robot later. A visual C#.NET Windows Application is developed for this purpose. C# language is chosen for the implementation of the project since project development environment is easy to use, coding in C# language is functional, and C# is one of the most popular object oriented programming language.

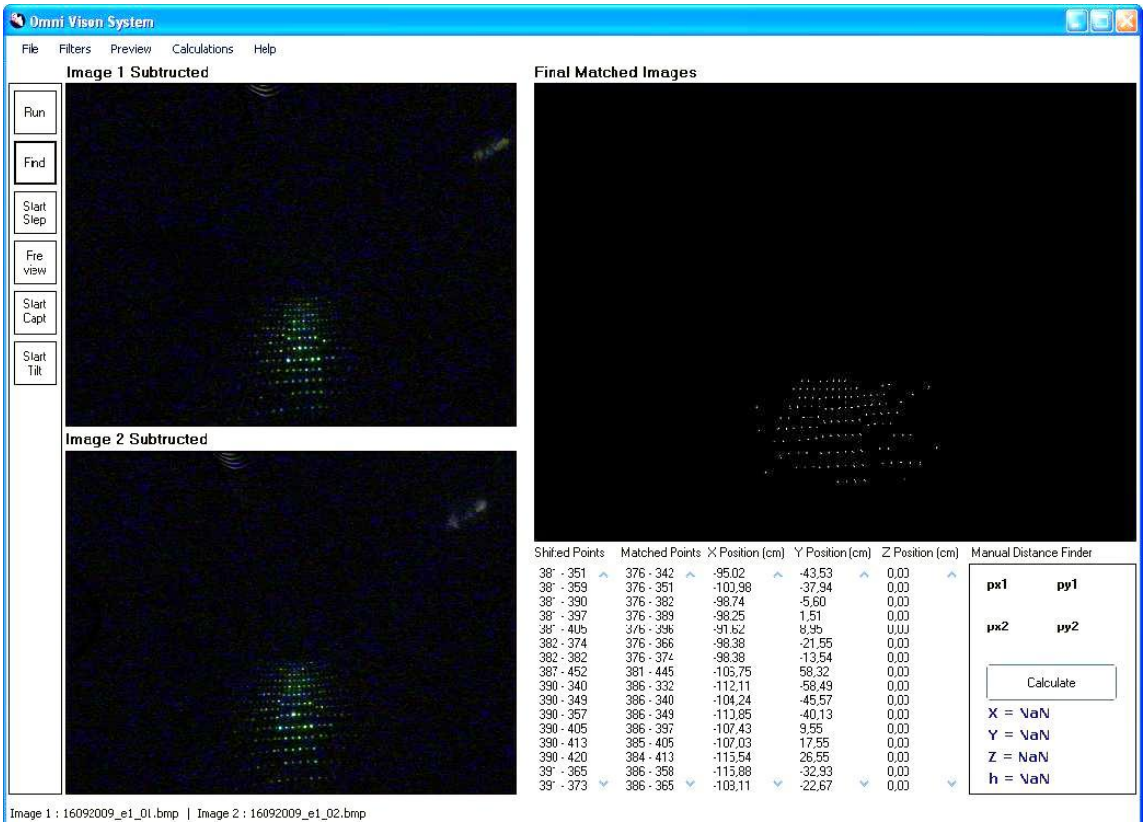

Figure 4.12 GUI of the developed software.

The class diagram of the developed software program in C# is given in Figure 4.13.

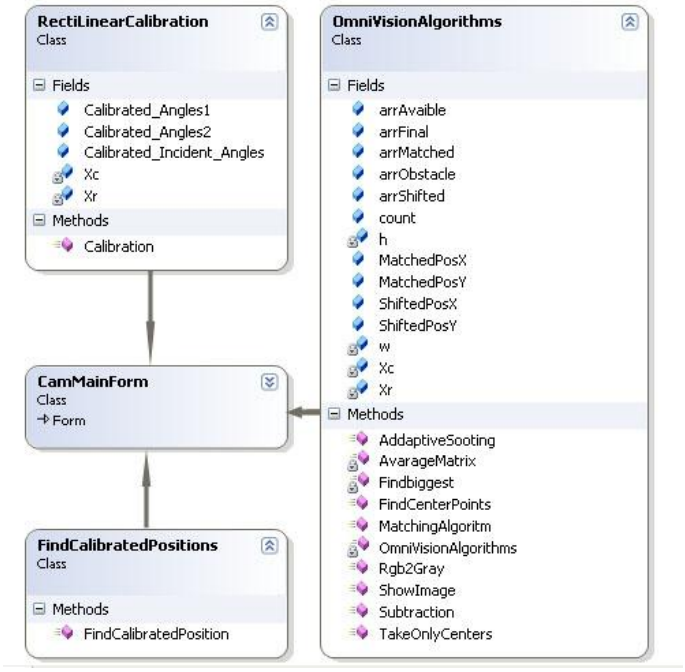

Figure 4.13 Class diagram of the developed software.

There are four main classes in the software. `CamMainForm` is the main class of the program. All the forms, menus and other controls are included in this class. `CamMainForm` class attributes and methods are not mentioned here because these method and controls are used only for graphical interface, menus and form controls. Overview of the classes are given in Table 4.1, Table 4.2 and Table 4.3.

Table 4.1 OmniVisionAlgorithms class overview.

OmniVisionAlgorithms class	
Subtraction Method	Subtraction method takes two image arguments and returns a subtracted image value then the results converted to a two dimensional array value for further calculations. After the image pairs taken from the environment by using the imaging system, CamMainForm calls Subtraction method in order to subtract mask image from the live image and gets the difference image.
Rgb2Gray method	Rgb2Gray takes a two dimensional array argument and returns the array value. This method in OmniVisionAlgorithms class converts the difference image to the grayscale difference image.
AddaptiveSmooting method	AddaptiveSmooting method takes a 2 dimensional image array as an argument and returns the same array value. AddaptiveSmooting method used for decreasing the distortion and noise on the 2 dimensional image array. This method uses the AverageMatrix method in OmniVisionAlgorithms class continuously because this smoothing operation is done for each 21x21 pixel window.
AverageMatrix method	AverageMatrix method takes 2 dimensional array values and calculates the average of these pixels for AddaptiveSmooting method.
FindCenterPoints method.	FindCenterPoints method takes a two dimensional image array as an argument and returns the same array. After Smoothing process This method finds the center of laser points by using the algorithm given in Figure 16. In order to obtain the brightest pixel in the 8x8 window FindCenterPoints method uses the Findbiggest method in OmniVisionAlgorithms class continuously.
Findbiggest method	Findbiggest method takes 2 dimensional array values and finds the highest gray level of these pixels for FindCenterPoints method.
TakeOnlyCenters method	TakeOnlyCenters method takes 2 dimensional array values and returns the same array. This method set a pixel gray level 0 (black) if that pixel's gray level value is smaller than 225 (white).
MatchingAlgorithm method	MatchingAlgorithm method takes two arguments and returns the calculated results of Matched laser Points, available passing areas at the ground level and obtained the laser points over an obstacle in the image. This method sets all the public fields in the class.
ShowImage method	ShowImage method takes 2 dimensional array values and returns a grayscale bitmap image value. This method is used to display results

Table 4.2 RectilenearCalibration class overview.

RectiLinearCalibration class	
Calibration Method	This method is called in main form load in order to calibrate distances. Calibration method doesn't take any arguments. In order to obtain 3D positions of the laser points, Calibration method is used to calculate necessary calibrated angle values.

Table 4.3 FindCalibratedPositions class overview.

FindCalibratedPositions class	
FindCalibratedPosition Method	FindCalibratedPosition method takes 7 arguments and returns the 3D position of the matched pixel. Arguments are row and column values of a pixel in the first matched image, row and column values of a pixel in the second matched image and Calibrated C1, C2, C3 angle values for that row and column positions.

CHAPTER FIVE
EXPERIMENTS

5.1 Preliminary Studies

In the initial phase of the project and before supply of the planned equipments in the project, a vision system is prepared by using the manually prepared equipments and necessary programs are coded in MATLAB in order to use developed algorithms on the vision system. The results taken from the first vision system are not adequate, so the new vision system is constructed by using the new equipments supplied from the project.

The first experiment performed in the imaging system was carried out with two mirror and camera systems placed 150 mm distance from each other is given in Figure 5.1. By using this system, *live* (Figure 5.1a) and *mask* (Figure 5.1c) images were obtained from the taken images. After that, laser spots on the images were determined by using developed algorithms as shown in Figure 5.1b and Figure 5.1d.

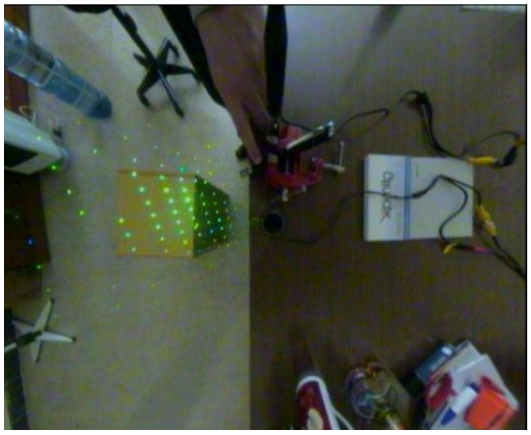

(a) *Live* image on camera 1

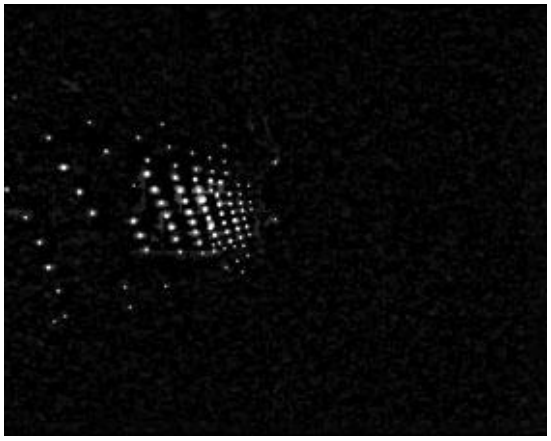

(b) Laser Points on the *live* image for camera 1

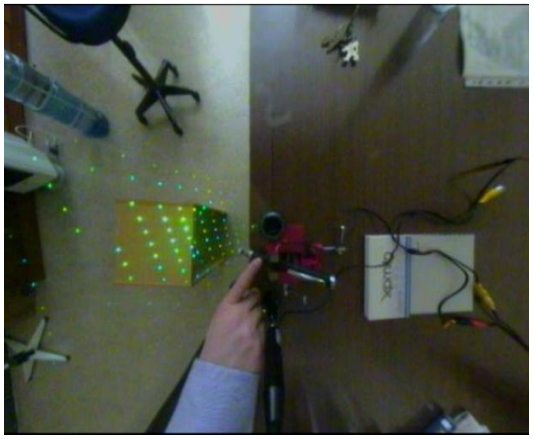

(c) Live image on camera 2

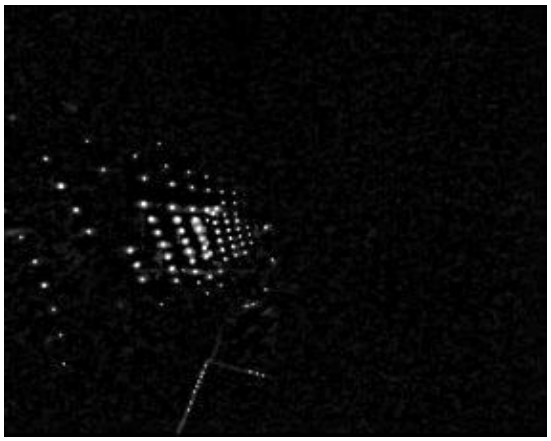

(d) Laser Points on the live image for camera 2

Figure 5.1 Determined laser spots from the image pairs.

Since the matching algorithms of two images were under development, to detect possible errors while determining the positions of the laser points, 6 control points and their (*X, Y, Z*) real positions according to the vision system was measured manually. Control points on the *live* image for the camera 1 are given on Figure 5.2.

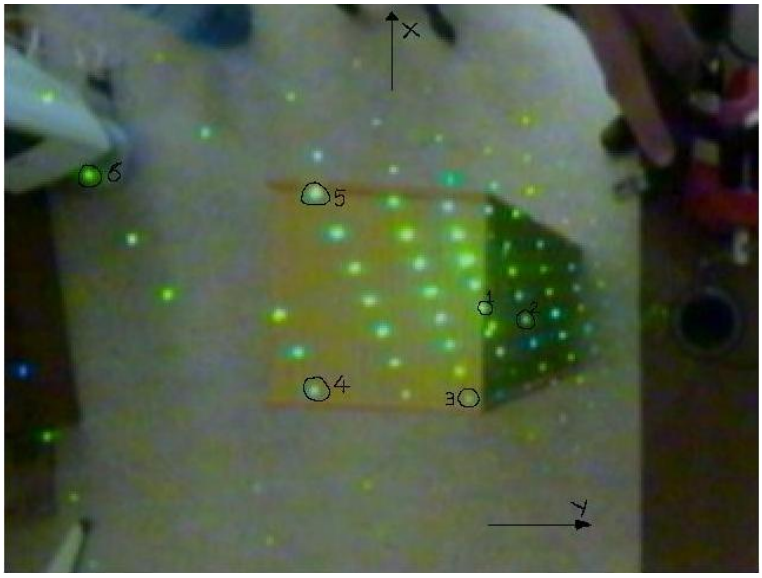

Figure 5.2 Selected points on *live* image from the imaging system.

Row and column (*x, y*) values belonging to the control points were determined for each mirror, and the positions of each point was calculated by using the software program prepared for this purpose. Obtained results were compared with measured values and error rates were determined (Table 5.1).

Table 5.1 Calculated locations and error rates of some points

# of Point	**Locations in the image, pixel**				**Calculated distances in the environment, cm**			**Measured distances in the environment, cm**			**Error rate, ± (%)**		
	Mirror-1		**Mirror-2**										
	x	***y***	***x***	***y***	***CX***	***CY***	***CZ***	***MX***	***MY***	***MZ***	***EX***	***EY***	***EZ***
1	238	242	271	239	3.00	-44.00	48.00	3.00	-46.00	55.00	**0.00**	**-4.35**	**-12.73**
2	243	260	263	256	2.00	-60.00	81.00	2.00	-63.00	95.00	**0.00**	**-4.76**	**-14.74**
3	276	235	309	232	-15.00	-49.00	49.00	-15.50	-51.50	55.00	**-3.23**	**-4.85**	**-10.91**
4	273	170	306	166	-13.00	-79.00	49.00	-13.50	-84.00	55.00	**-3.70**	**-5.95**	**-10.91**
5	189	170	222	168	25.00	-75.00	46.00	26.00	-80.00	55.00	**-3.85**	**-6.25**	**-16.36**
6	182	74	202	72	46.00	-194.00	76.00	48.00	-215.00	92.00	**-4.17**	**-9.77**	**-17.39**

***CX*, *CY*, *CZ*:** Calculated Distance; *MX*, *MY*, *MZ*: Measured Distance; *EX*, *EY*, *EZ*: Error Rate

As a result of this calculation, the largest error rates are -4.17% in *X-axis* and -9.77% in *Y-axis* for point 6. Point 6 is placed on an obstacle and far from the vision system. Near the vision system, error rates are smaller than the point 6. Therefore, it is assumed that the error rate increases with the distance from the vision system.

The error rate in the *Z-axis* is -17.39% in point 6 again. It is relatively higher than the *X* and *Y* axes. The higher error rate on the *Z-axis* is predictable because the error rate on the *Z-axis* depends on the errors in *X* and *Y* axes.

The general reasons for these errors are thought to be mechanical and caused by the movement of the vision system, hardware structure of the vision system platform, the mechanical problems experienced to adjust height of the camera-mirror pairs, and the difficulties about parallelization of the mirror axes.

5.2 Studies After Matching Laser Points

After preliminary studies carried out in the prepared imaging system, elimination of errors caused by hardware problems is begun to be studied, mechanical arrangements was made and software arrangements were done for fixing the calculation problems. At the end of these arrangements, experiments were started over the prepared vision system and system performance and error rates were determined.

5.2.1 Studies with a Single and High Obstacle

In this first experiment, a single and high obstacle was placed center of the vertical axis and in front of the vision system as shown in Figure 5.3. By using the vision system, *live 1* (Figure 5.3a) and *live 2* (Figure 5.3b) images were obtained.

Two separate images were evaluated in the experiment. All the laser points on the floor and on the obstacle were placed in the first image as shown in Figure 5.3c. The laser points on the obstacle were lined up more rarely than the points on the floor. The distance between the laser points on the front side of the obstacle was more than the other points on the floor. The lines of the laser points on the obstacle were parallel and had a particular distance to each other. In order to determine obstacles and possible passing areas in the environment, points on the obstacles were removed

from the matching image as shown in Figure 5.3d. So that, the points at the ground level image were obtained for a safe move.

Obtained results are given on Table 5.2. During preliminary studies, the direction of the dual mirror-camera system standing was called *X-axis*, but after matching arrangements this direction is called *Y-axis*. So that, the *X* and *Y* axes in Table 5.1 will be corresponding to *Y* and *X* axes in Table 5.2, Table 5.3 and Table 5.4.

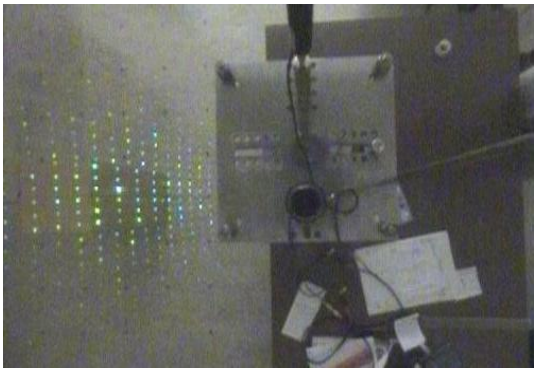

(a) *Live1* image

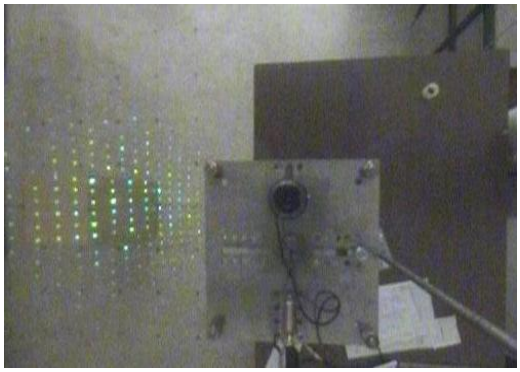

(b) *Live2* image

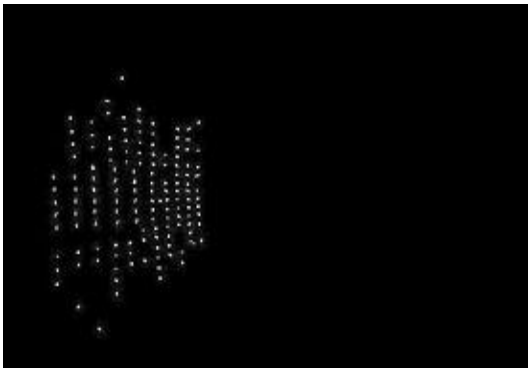

(c)Matched all pixels

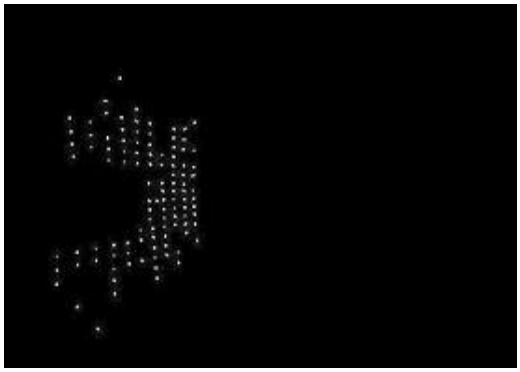

(d) Matched pixels without obstacle

Figure 5.3 Images of a single and high obstacle.

Table 5.2 Calculated locations and error rates of the points for a single and high obstacle.

# of Point	Locations in the image, pixel				Calculated distances in the environment, cm			Measured distances in the environment, cm			Error rate, ± (%)		
	Mirror-1		Mirror-2										
	x	***y***	***x***	***y***	***CX***	***CY***	***CZ***	***MX***	***MY***	***MZ***	***EX***	***EY***	***EZ***
1	400	405	396	398	-122.40	9.90	121.50	-120.00	10.50	117.00	**2.00**	**-5.71**	**3.85**
2	414	381	410	372	-117.10	-13.10	103.00	-120.00	-12.50	106.00	**-2.42**	**4.80**	**-2.83**
3	413	422	409	415	-131.90	26.80	117.00	-120.00	24.50	107.00	**9.92**	**9.39**	**9.35**
4	445	427	442	417	-131.10	25.40	92.20	-120.00	27.00	87.00	**9.25**	**-5.93**	**5.98**
5	483	388	483	375	-133.30	-5.30	75.10	-131.00	-5.40	77.00	**1.76**	**-1.85**	**-2.47**
6	481	432	481	420	-131.90	24.30	75.10	-130.50	24.00	77.00	**1.07**	**1.25**	**-2.47**

***CX*, *CY*, *CZ*:** Calculated Distance; *MX*, *MY*, *MZ*: Measured Distance; *EX*, *EY*, *EZ*: Error Rate

As a result of this calculation, the largest error rates in *X, Y, Z* axes are respectively 9.92%, 9.39% and 9.35% at point 3. Although, point 3 have the same *X-axis* value with points 1 and 2 and nearly same perpendicular distance from the vision system, this point is placed the second highest position from the vision system and again the second most remote location from the center of the image plane.

The second largest error rates for all *X, Y, Z* axes are respectively 9.25%, -5.93% and 5,98% at point 4. Besides the smallest error rates for all *X, Y, Z* axes are respectively 1.07%, 1.25% and -2.47% at point 6. This point is more remote than point 3 and 4 on *X-axis*, nearly same with point 3 and nearer than point 4 on *Y-axis*, and the nearest on *Z-axis*.

The results (*x, y* and *z* coordinates) obtained from the calculations were displayed through a software package, and 3D shape of objects in the environment were obtained as shown in Figure 5.4. For this purpose, to interpolate calculated points the Nearest Neighbor Method is used with a 150mm radius. The shape of the object could not be drawn properly because of the distance increment between the consecutive laser points placed on the floor and on the obstacle, the limited number of laser points striking the object, and possible errors in measurement.

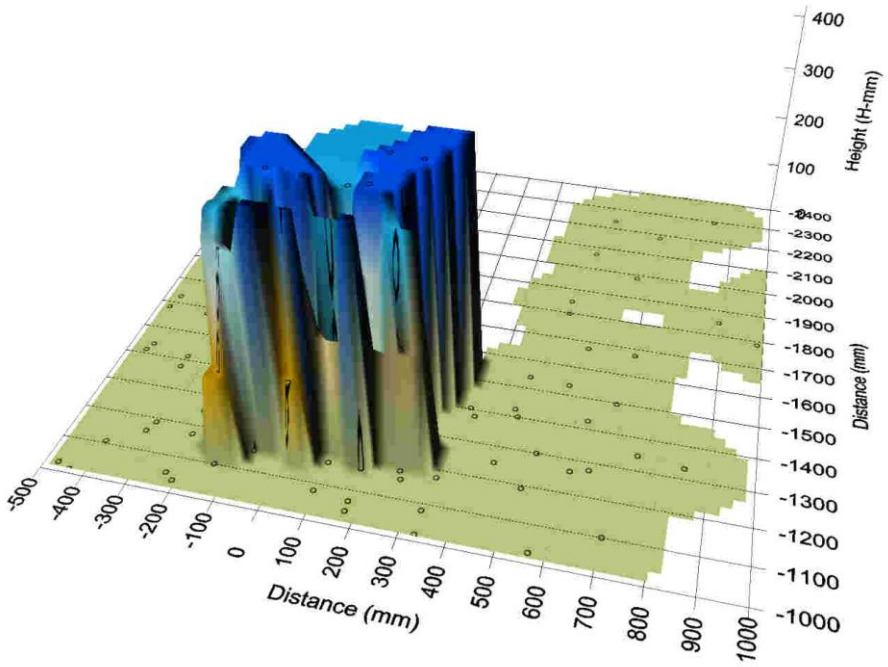

Figure 5.4 3D view of a single and high obstacle.

The error rates of the imaging system were examined in terms of distance. It was seen that the error rates of the points are not dependent on the *X* and *Y* axes, but dependent on the distance on *Z-axis*. Moreover, in order to investigate the relations of error rates with each other, the vertical distances of the points from the image plane, on *Z-axis*, were also examined (Figure 5.5).

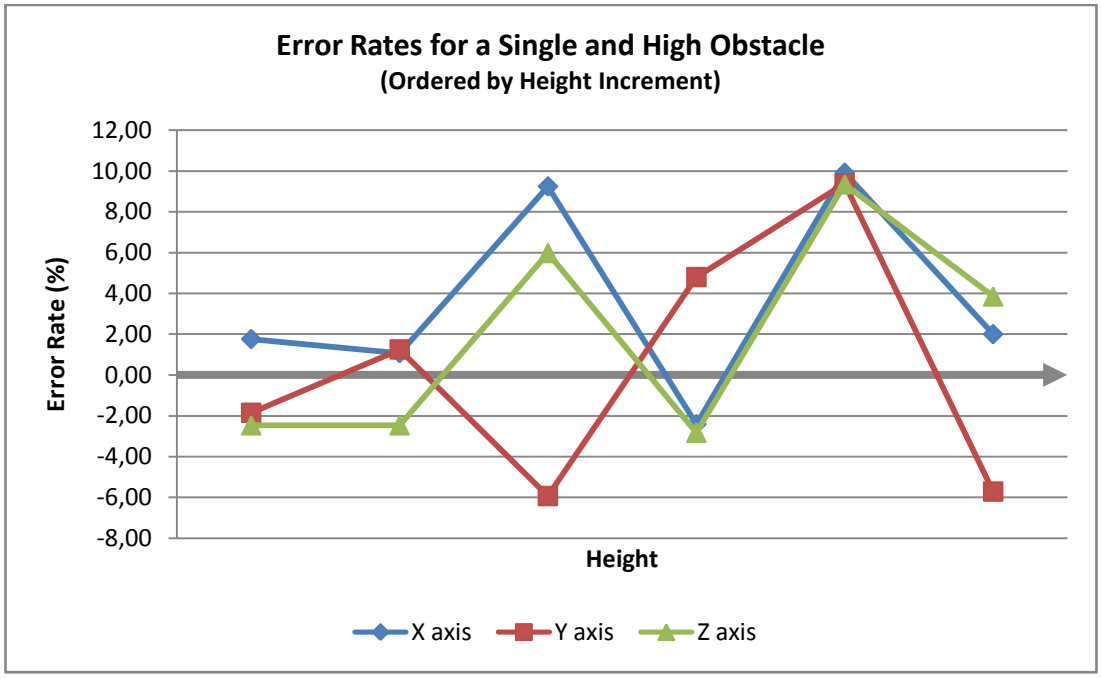

Figure 5.5 Error rates for a single and high obstacle.

According to these values, it can be seen that there is a relation between the error rates on *X* and *Z* axes, but there is only a partial relation between *Y-axis*.

5.2.2 Studies with Two Obstacles

In the second experiment two obstacles were placed in the environment. They were placed equal distance from the vertical axis which is perpendicular to the vision system's center as shown in Figure 5.6. By using the vision system, *live 1* (Figure 5.6a) and *live 2* (Figure 5.6b) images were obtained.

Two separate images were evaluated in the experiment as in the first experiment. All the laser points and obstacles are placed in the environment as shown in Figure 5.6c. The laser points on the obstacle were lined up more rarely than the points on the floor. The distance between the laser points on the front side of the obstacle was more than the lines of the laser points on the floor. The lines of the laser points on the obstacle were parallel and had a particular distance to each other.

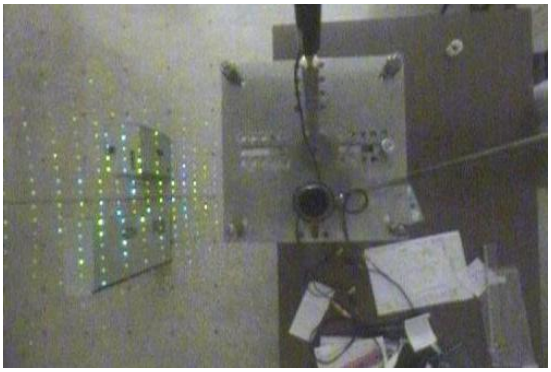

(a) *Live1* image

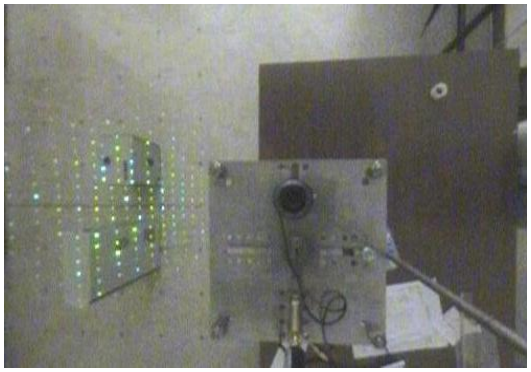

(b) *Live2* image

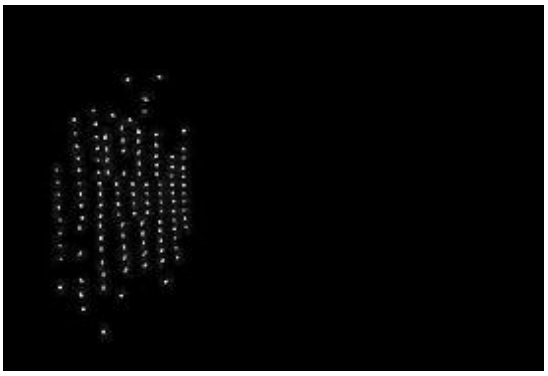

(c) Matched all pixels

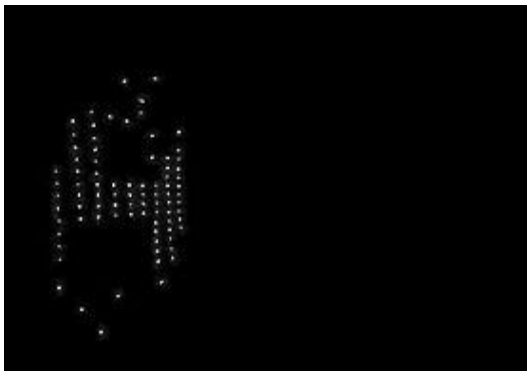

(d) Matched pixels without obstacles

Figure 5.6 Images of two obstacles.

In order to determine obstacles and possible passing areas in the environment, points on the obstacles were removed from the matching image as shown in Figure 5.6d. So that, the points at the ground level image were obtained for a safe move.

Obtained results are given on Table 5.3. During preliminary studies, the direction of the dual mirror-camera system standing was called *X-axis*, but after adjustment in matching this direction is called *Y-axis*.

Table 5.3 Calculated locations and error rates of the points for two obstacles.

# of Point	Locations in the image, pixel				Calculated distances in the environment, cm			Measured distances in the environment, cm			Error rate, ± (%)		
	Mirror-1		Mirror-2										
	x	***y***	***x***	***y***	***CX***	***CY***	***CZ***	***MX***	***MY***	***MZ***	***EX***	***EY***	***EZ***
1	415	380	411	371	-118.10	-14.00	103.00	-120.00	-14.50	106.00	**-1.58**	**-3.45**	**-2.83**
2	415	344	412	336	-129.80	-50.80	113.30	-120.00	-47.50	106.00	**8.17**	**6.95**	**6.89**
3	430	380	427	370	-124.70	-13.30	97.10	-120.00	-13.00	106.00	**3.92**	**2.31**	**-8.40**
4	445	339	443	329	-138.10	-48.40	97.00	-134.00	-47.00	96.50	**3.06**	**2.98**	**0.52**
5	482	454	481	443	-133.60	39.40	75.70	-127.50	40.00	75.50	**4.78**	**-1.50**	**0.26**
6	443	446	441	437	-128.90	40.60	91.80	-120.50	38.00	90.00	**7.42**	**6.84**	**2.00**

***CX*, *CY*, *CZ*:** Calculated Distance; *MX*, *MY*, *MZ*: Measured Distance; *EX*, *EY*, *EZ*: Error Rate

The largest error rates for *X* and *Y* axes are respectively 8.17% and 6.95% at point 2, and for *Z-axis* is -8.40% at point 3 as shown from the table. Although these points have the same *x* and *z* values, the y values are different from each other.

The smallest error rate for X-axis is -1.58% at point 1, and for the *Y* and *Z* axes are -1.50% and 0.26% at point 5. Point 5 have the lowest error rate 0.26% all of these points, and the closest vertical point to the vision system.

3D shapes of objects in the environment were obtained from the calculated positions by using software package (Figure 5.7). The location of these two objects in the environment can be clearly seen, but the objects were not placed exactly symmetrical according to images taken from cameras. Although all transactions are based on the positions of objects in the mirrors, in order to find the locations of the objects real coordinates are used in calculations. Therefore, the mirror images and the real images are symmetrical to each other.

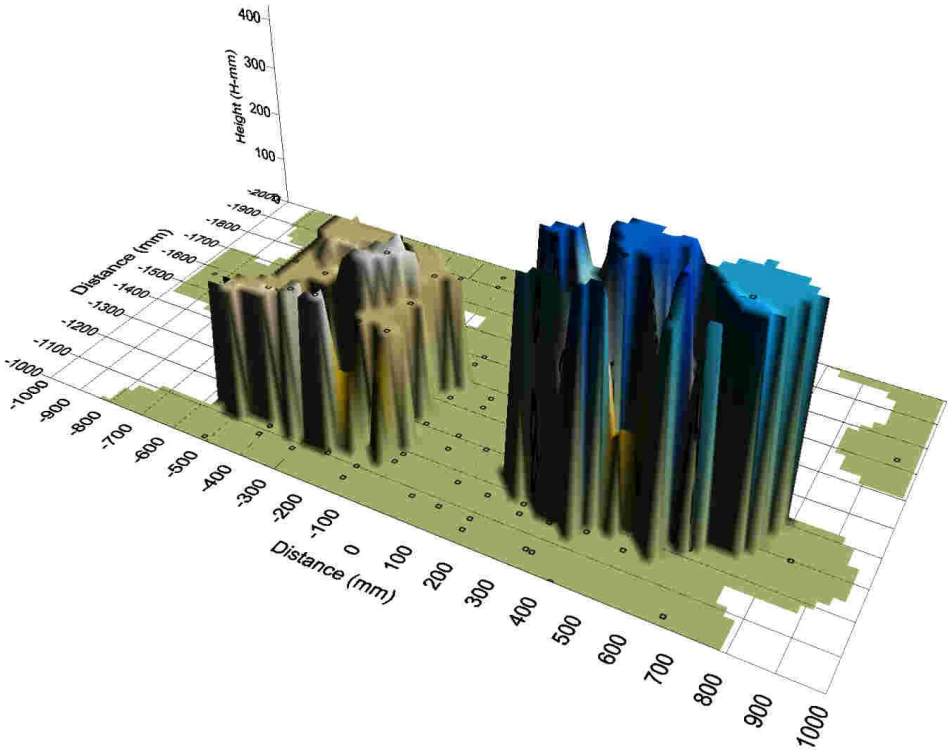

Figure 5.7 3D views of two obstacles.

The error rates of the imaging system were examined in terms of distance, like in the image of single and high obstacle, the error rates of the points were not dependent on the *X* and *Y* axes, but dependent the distance on *Z*-axis. Moreover, in order to investigate the relations of error rates with each other, the vertical distances of the points from the image plane, on *Z-axis*, were also examined in Figure 5.8.

According to these values, it can be seen that the error rates caused by the errors when obtaining the locations, were independent from the axes, but the error rates occurred on the axes are dependent on each other. An error on one axis directly effects the amount of the error on the other axis. This situation is especially apparent for the *X* and *Y* axes.

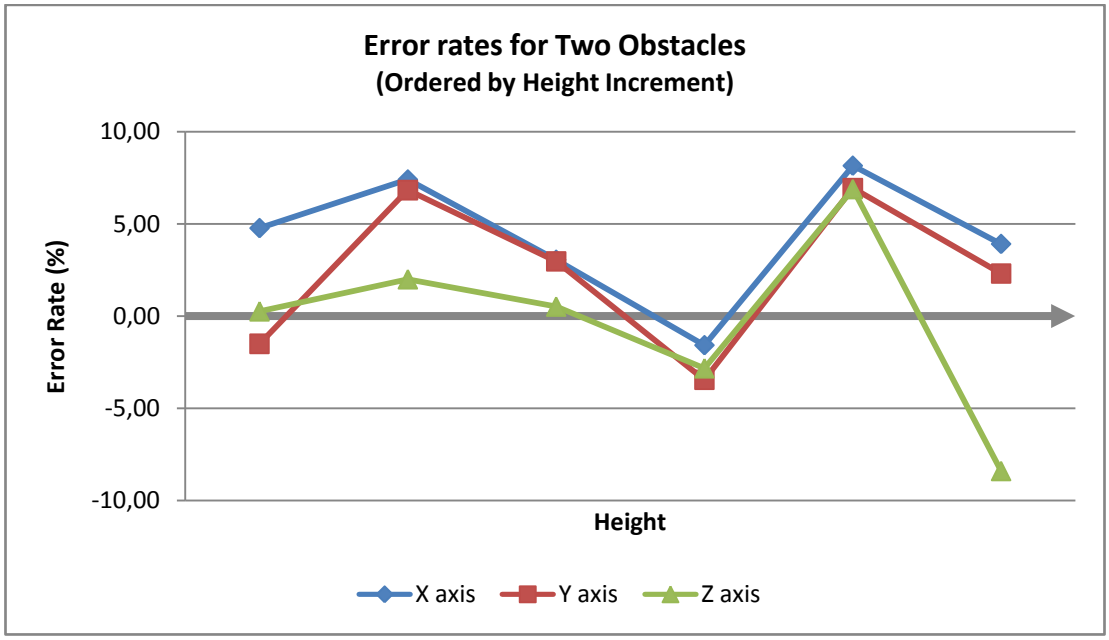

Figure 5.8 Error rates for two obstacles.

5.2.3 Studies with a Small Single Obstacle

In this third experiment a small obstacle was placed center of the vertical axis and in front of the vision system as shown in Figure 5.9. By using the vision system, *live 1* (Figure 5.9a) and *live 2* (Figure 5.9b) images were obtained.

Two separate images were evaluated in the experiment. All the laser points and obstacles were placed in the environment in the first image as shown in Figure 5.9c. The laser points on the obstacle were lined up more rarely than the points on the floor. The distance between the laser points on the front side of the obstacle is larger than the other lines consisting of the laser points on the ground. The lines of the laser points on the obstacle were parallel and had a particular distance to each other. In order to determine obstacles and possible passing areas in the environment, points on the obstacles were removed from the matching image as shown in Figure 5.9d. So that, the points at the ground level image were obtained for a safe move. Obtained results are given on Table 5.4.

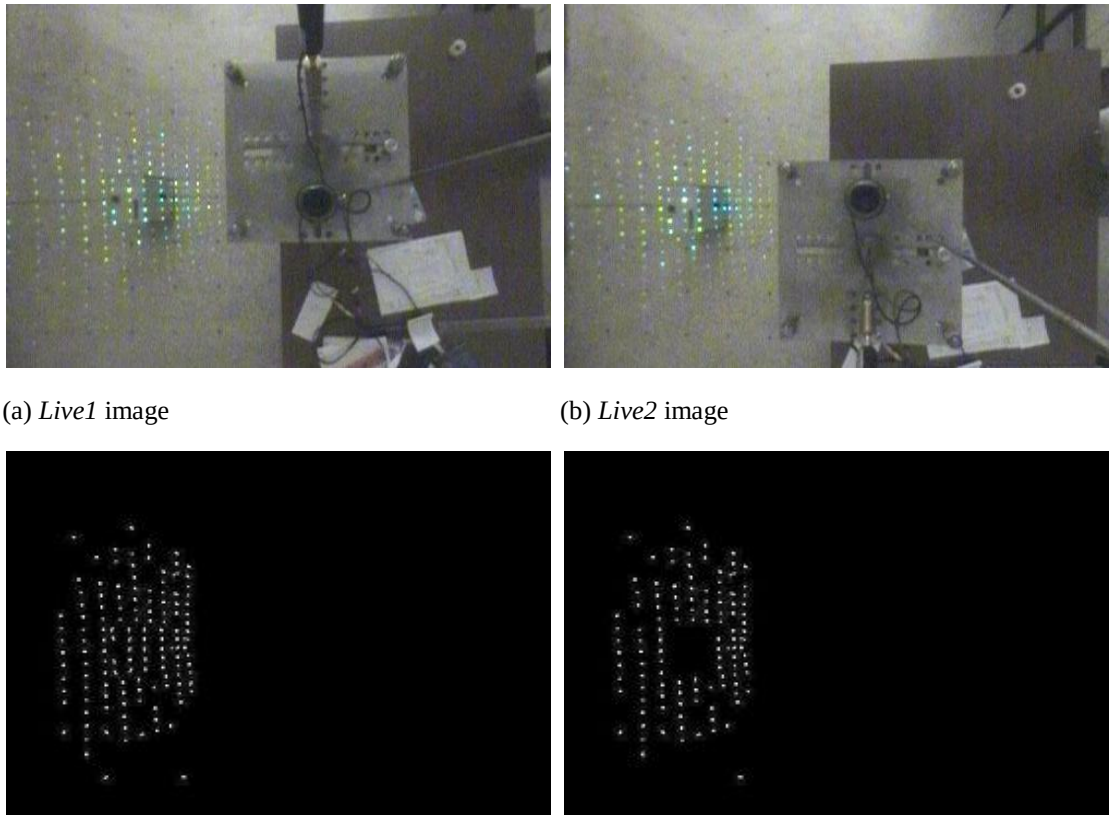

(a) *Live1* image (b) *Live2* image

(c) Matched all pixels (d) Matched all pixels without obstacle

Figure 5.9 Image of a small single obstacle.

Table 5.4 Calculated locations and error rates of the points for a single and small obstacle.

# of Point	Locations in the image, pixel				Calculated distances in the environment, cm			Measured distances in the environment, cm			Error rate, ± (%)		
	Mirror-1		Mirror-2										
	x	***y***	***x***	***y***	***CX***	***CY***	***CZ***	***MX***	***MY***	***MZ***	***EX***	***EY***	***EZ***
1	414	389	411	380	-118.40	-6.00	104.20	-120.00	-6.20	106.00	**-1.33**	**-3.23**	**-1.70**
2	413	423	409	415	-123.50	26.00	109.60	-120.00	25.00	105.50	**2.92**	**4.00**	**3.89**
3	438	340	435	332	-148.70	-53.50	109.50	-156.00	-57.50	117.00	**-4.68**	**-6.96**	**-6.41**
4	445	474	444	471	-173.80	84.20	122.10	-166.50	80.00	117.00	**4.38**	**5.25**	**4.36**
5	456	397	455	388	-146.80	1.10	96.30	-145.00	1.10	96.50	**1.24**	**0.00**	**-0.21**
6	464	396	463	390	-174.90	0.20	109.40	-184.00	0.20	117.00	**-4.95**	**0.00**	**-6.50**

***CX*, *CY*, *CZ*:** Calculated Distance; *MX*, *MY*, *MZ*: Measured Distance; *EX*, *EY*, *EZ*: Error Rate

The largest error rates for *X* and *Z-axis* are respectively -4.95% and -6.50% at point 6 and for *Y-axis* is -6.96% at point 3 is shown from the table. Both these points have same height values, and point 6 is placed nearly on *Y-axis*.

The smallest error rates for *X, Y, Z* axes are respectively -4.95%, 0.00% and -6.50% at point 5. Point 5 and point 6 have zero position error on Y-axis.

3D shape of objects in the environment was obtained from the calculated positions by using software package as shown in Figure 5.10.

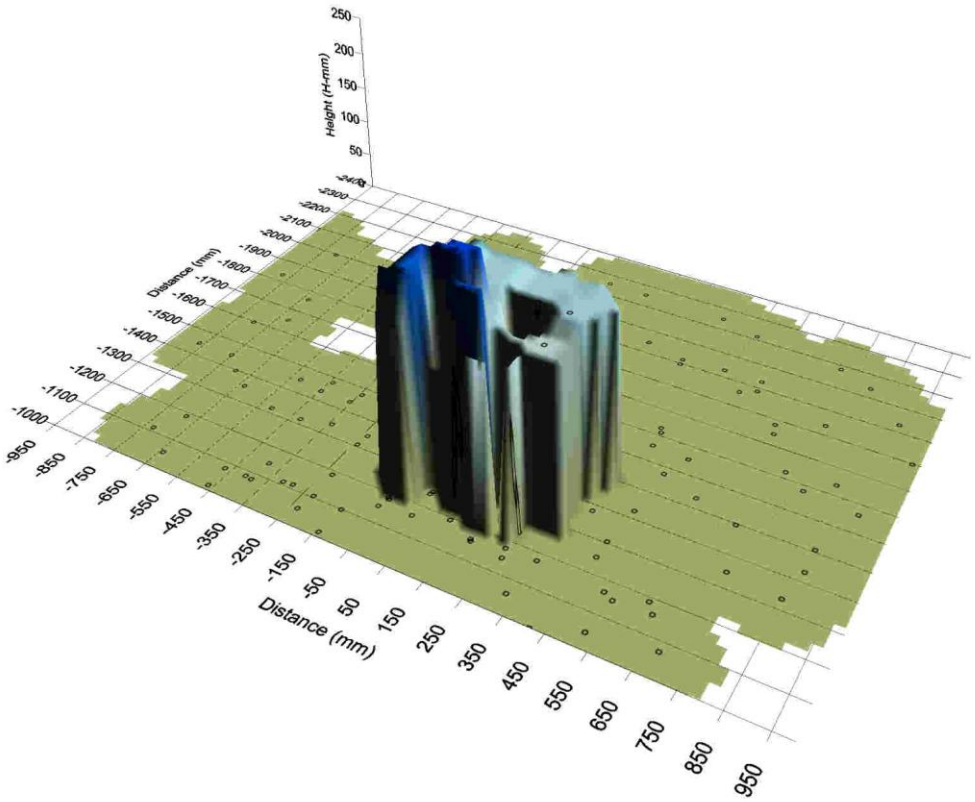

Figure 5.10 3D view of a single and small image.

The error rates of the imaging system were examined in terms of distance, like in the previous experiments. It was seen that the error rates of the points were not dependent on the *X* and *Y* axes, but dependent on the distance on *Z-axis*. However, the dependency of this error rate on *Z-axis* was decreased by the increment of distance. When the change in the error, depending on the distance to the axis, was taken into account, error rates vary irregularly by the increment of distance depending on *X* and *Z* axes. But this situation was different for the Y-axis. The error rate increased regularly depending on the increment of distance.

In order to investigate the relations of error rates of the imaging system, in terms of distance, the vertical distance, depending on the *Z-axis*, from the imaging plane are examined as shown in Figure 5.11.

Figure 5.11 Error rates for a single small obstacle.

According to these values, it can be seen that the error rates caused by the errors when obtaining the locations, were independent from the axes, but the error rates occurred on the axes are dependent to each other. An error on one axis directly effects the amount of the error on the other axis. This situation is apparent for the *X*, *Y* and *Z* axes.

CHAPTER SIX
CONCLUSION

In this study, an omni-directional vision system was prepared to obtain the 3D structure of the current environment. This vision system consists of two rectilinear mirrors and two CCD cameras and a fiber grating laser device in order to obtain a dot-matrix laser pattern.

Determining the obstacles and obtaining the 3D distances of the current environment is very significant for mobile robot implementations. In order to obtain the locations of the obstacles in the environment, 3D distances of the laser points are used in the vision system. Moreover, a mathematical model was prepared for calculating the laser point's positions.

Prepared vision system and models were tested by using three different types of obstacles. First experiment with a single and high obstacle, second experiment with two obstacles and third experiment with a single small obstacle were investigated and results are compared.

Although coordinate calculations have 17% error rates especially in the height values, these error rates are under 10% in vertical axes. After using the developed mathematical model for matching process, the error rates are decreased under 10% values for all axes.

The smallest and largest error rates for *X-axis* are respectively 1.07% and 9.92%. The evaluations of error rates on *Y-axis* the smallest and the largest error rates are respectively 0.00% and 9.39%.The evaluations of error rates on *Z-axis* smallest and the largest error rates are respectively 0.21% and 9.35%.

Error rates are increased by the increment of the distance between the laser point and the vision system. However, the error rate for *Z-axis* is not directly dependent to the distance. The main reasons of errors were reflection errors on the mirrors,

sensitivity of the refractive lens used in the system, alignment of the mirror-camera pairs and limitation of the image resolution.

In order to minimize the error rate of calculated distances, the resolutions of the cameras should be increased and the alignment system of the mirror-camera pairs will be improved. Moreover, to minimize the reflection errors on the mirrors, developed algorithms used for the laser spots on the image should be improved. In the future, after the improvements, this system may be used in mobile robot applications.

REFERENCES

Baker, S., & Nayar, S. (1999). A theory of single-viewpoint catadioptric image formation. *International Journal of Computer Vision, 35* (2), 175-196.

Chang Y., Kuwabara H., & Yamamoto Y. (July 2008). Novel Application of a Laser Range Finder with Vision System for Wheeled Mobile Robot. *IEEE/ASME International Conference on Advanced Intelligent Mechatronics*, 280-285.

Duan Z., & Cai Z. (July 2008). Robust Simultaneous Localization and Mapping Based on Laser Range Finder with Improved Adaptive Particle Filter. *Control and Decision Conference, (CCDC),* 2820-2824.

Gasparri, A., Panzieri S., Pascucci F., & Ulivi G. (April 2007) A Hybrid Active Global Localisation Algorithm for Mobile Robots. *IEEE International Conference on Robotics and Automation,* 3148-3153.

Gluckman, J., Nayar, S. K., & Thoresz, K. J. (1998). A real-time omnidirectional and panoramic Stereo. *DARPA Image Understanding Workshop (IUW),* 309-313.

Gluckman, J., & Nayar, S. K. (1999). Planar catadioptric stereo: geometry and calibration. *IEEE Conference on Computer Vision and Pattern Recognition (CVPR),* (1), 22-28.

Gluckman, J., & Nayar, S. K. (2002). Rectified catadioptric stereo sensors. *IEEE Transastions on Pattern Analysis and Machine Intelligence, 24* (2), 224-236.

Habib, M. K. (January 2007). Fiber-grating-based vision system for real-time tracking, monitoring and obstacle detection. *IEEE Sensors Journal, 7* (1), 105-121.

Kriegman, D.J., Triend, E., & Binford T.O. (December 1989). Stereo Vision and Navigation in Buildings for Mobile Robots. *IEEE Transactions on Robotics and Automation, 5,* 792-803.

Kweon, G., Hwang-Bo, S., Kim, G., Yang, S., & Lee, Y. (2006). Wide-angle catadioptric lens with a rectilinear projection scheme. *Applied Optics, 45* (34), 8659-8673.

Nakazawa, K., & Suzuki, C. (1991). Development of 3-D robot vision sensor with fiber grating: fusion of 2-D intensity image and discrete range Image. *International Conference on Industrial Electronics, Control and Instrumentation, (IECON '91), 3,* 2368-2372.

Nayar, S. K. (1997). Catadioptric omnidirectional camera. *Proceeding of IEEE Conf. On Computer Vision and Pattern Recognition,* 482-488.

Nene, S. A., & Nayar, S. K. (January 1998). Stereo with Mirrors. *Proceedings of the 6th International Conference on Computer Vision,* 1087-1094.

Ohya, A., Shoji, & E., Yuta, S. (1994). 3-D range Sensor using fiber grating for recognition of autonomous mobile robot's passage space. *Intelligent Robots and Systems '94, Advanced Robotic Systems and the Real World' IROS '94. Proceedings of the IEEE/RSJ/GI International Conference 3,* 1759-1763.

Svoboda, T., Pajdla, T. & Hlavac V. (2002). *Omnidirectional Vision.* Retrived October 11, 2009 from http://cmp.felk.cvut.cz/demos/Omnivis/.

Yamaguchi, J., & Nakajima, M. (November 1990). A 3D shape identification system using a fiber grating vision sensor. *Industrial Electronics Society, IECON '90, 16th Annual Conference of IEEE, 1*, 507-511.

Wang, J.H., & Hsiao C.P. (1996), Stereo matching by neural network that uses Sobel Feature data. *IEEE International Conference on Neural Networks, 3*, 1801-1806.

Zhang, Z**.** (2000). A flexible new technique for camera calibration. *IEEE Transactions on Pattern Analysis and Machine Intelligence*, *22* (11), 1330-1334.